Chapter 11

Crystal Growth by Electrodeposition with Supercritical Carbon Dioxide Emulsion

Masato Sone, Tso-Fu Mark Chang and
Hiroki Uchiyama

Additional information is available at the end of the chapter

http://dx.doi.org/10.5772/54070

1. Introduction

1.1. Electroplating with supercritical carbon dioxide emulsion

1.1.1. Introduction

1.1.1.1. Supercritical Carbon Dioxide

A supercritical fluid (SCF) is any substance at a temperature and pressure above its critical point, as shown in Fig. 1, where distinct liquid and gas phases do not exist [1]. It can effuse through solids like a gas, and dissolve materials like a liquid. In addition, close to the critical point, small changes in pressure or temperature result in large changes in density, allowing many properties of a SCF to be fine-tuned between a gas and a liquid. SCFs are suitable as a substitute for organic solvents in a range of industrial and laboratory processes.

CO_2 is non-polar, combining with the low surface tension property when it is in supercritical state; it is often used in extraction of organics in the food industries [2]. The extremely low surface tension also makes supercritical CO_2 (sc-CO_2) an ideal medium in drying of nano-porous structures [3]. CO_2 is non-toxic, and the critical point is relatively low when comparing with the other solvents, therefore, sc-CO_2 is an important commercial and industrial solvent. Critical temperature pressure of sc-CO_2 are 304.5K and 7.39 MPa, respectively. Comparison for the critical conditions of some commonly used solvents is shown in Table 1.

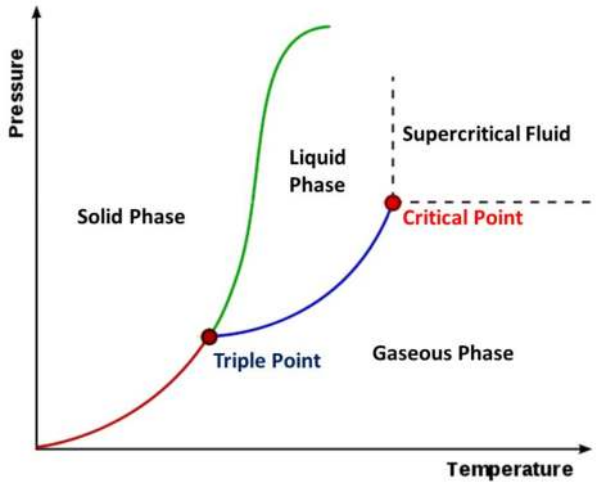

Figure 1. Phase diagram of a single substance.

Fluid	Critical Temperature (K)	Critical Pressure (MPa)
CO_2	304.1	7.39
NH_3	405.5	11.35
H_2O	647.3	22.12
n-Pentane	469.7	3.37
Toluene	591.8	4.10

Table 1. Critical conditions of commonly used solvents

1.1.1.2. Supercritical Carbon Dioxide Emulsion

Electrodeposition is a key technology for fabricating micro components used in micro-electro-mechanical systems (MEMS) [4,5]. Application of sc-CO_2 in electrodeposition process is believed to solve the problems encounter in miniaturization of the devices [6], such as reducing usage of organic solvents in the cleaning process, drying of the nano-structures after the electrodeposition process, and minimize problems caused by evolution of H_2. Evolution of H_2 is an inevitable size reaction when performing electrodeposition reaction with an aqueous electrolyte. H_2 gas bubbles adsorbed on the surface of cathode is one of the major causes for defects found in the electrodeposited materials [7]. CO_2 is non-polar, solubility of H_2 is high in CO_2 [8]. Therefore, desorption of H_2 gas bubbles from the surface of cathode could significantly enhanced in sc-CO_2.

http://dx.doi.org/10.5772/54070

However, electrical conductivity and metal salts solubility are both very low in sc-CO_2 [1], which are the basic requirements in electrochemistry. The limitations could be overcome by addition of a surfactant to form an emulsion composed of an aqueous electrolyte, sc-CO_2, and the surfactant [9,10]. Two types of the emulsion could be formed depending on the type and concentration of surfactant used and concentration of CO_2 in the system. One is H_2O in CO_2, where the continuous phase (CP) is CO_2 and the dispersed phase (DP) is H_2O. The other one is CO_2 in H_2O, where the CP is H_2O and the DP is CO_2 [11,12]. Structure of the DP in CO_2 in H_2O emulsion is similar to micelles in mixture of oil and water. CO_2 in H_2O emulsion is usually used for application in electrochemical reaction because the higher solubility of metal salts and electrical conductivity CO_2 in H_2O emulsion when compared with H_2O in CO_2 emulsion [11,12].

1.1.1.3. Electrodeposition with Supercritical Carbon Dioxide Emulsion (EP-SCE)

Surface smoothening, grain refinement, and hardness enhancement are the effects of applying sc-CO_2 emulsion (SCE) in electrodeposition of Ni [13-15]. Surface of the Ni films fabricated by electrodeposition with SCE (EP-SCE) is defect-free and pinhole free as shown in Fig. 2(a), and defects are found on the Ni films when only the aqueous electrolyte is used at ambient pressure as shown in Fig. 2(b) [13]. Ni films is electrodeposited with the aqueous electrolyte only at an elevated pressure, 42 MPa, to confirm the surface smoothening effect is not caused by the high pressure, and many defects are found on the Ni film as shown in Fig. 2(c). In order to further confirm the smooth surface is caused by SCE, emulsion made of n-hexane is studied [14]. Properties of n-hexane are considered to be close to sc-CO_2, such as electrical conductivity. Surface conditions of the Ni films fabricated by EP-SCE are much better than the Ni films fabricated by electrodeposition with n-Hexane. The results indicate that only emulsion made of sc-CO_2 is effective in increasing smoothness of the Ni films electrodeposited.

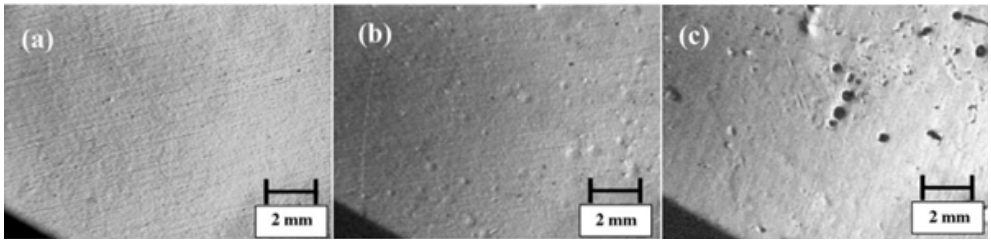

Figure 2. Ni films electrodeposited from (a)SCE, (b) the aqueous electrolyte only at atmospheric pressure and (c) the aqueous electrolyte only at 42 MPa.

For improvement in mechanical properties, grain refinement is believed to be the main cause as shown in Fig. 3 [15-17]. Ni films fabricated by EP-SCE are reported to have grain size in nano-scale. Because of the nano-grains, wear properties of the Ni films could be improved significantly [18]. Chung and Tsai proposed the grain refinement and

improvement in mechanical strength are also caused by C impurity in the Ni film from decomposition of CO_2 in the electrolyte; evidence of the C impurity is detected from X-ray photoelectron spectra [19].

Many studies have been reported on application of SCE in electrodeposition. However, additive such as brightener is often used in the electrolyte in these studies, and properties of the materials electrodeposited could be influenced by the additives [20,21]. Therefore, we studied and proposed a mechanism called periodic-plating-characteristic (PPC) to be the main cause for the effects observed in the metal films fabricated by EP-SCE. Physical properties of SCE are expected to affect the PPC and properties of the metal films electrodeposited, and physical properties of SCE could be controlled by varying experimental pressure, volume fraction of CO_2 and surfactant in the system. In this study, physical properties of SCE are adjusted to study the influence on PPC and properties of the Ni films electrodeposited.

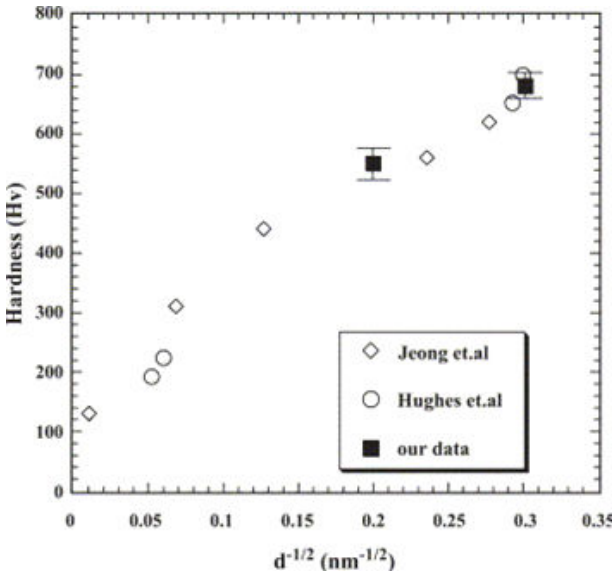

Figure 3. Effect of grain size on hardness.

1.1.2. Experimental section

1.1.2.1. Materials

CO_2 with a minimum purity of 99.9 % was used. Composition of the additive-free Watts bath was $NiSO_4 \bullet 6H_2O$ (300 g/l), $NiCl_2 \bullet 6H_2O$ (50 g/l), and H_3BO_3 (50 g/l). pH of the additive-free Watts bath was 3.31. A non-ionic surfactant, polyoxyethylene lauryl ether ($C_{12}H_{25}(OCH_2CH_2)_{15}OH$) was used to form the emulsion. Volume fraction of CO_2 with respect to the total volume of the reaction chamber and volume fraction of surfactant with

http://dx.doi.org/10.5772/54070

respect to the volume of the aqueous electrolyte were varied from 10 to 50 vol% and 0 to 2.0 vol%, respectively. Cu plates with width and length at 1.0X2.0 cm^2 were used as the working substrate, and Ni plates with width and length at 1.0X2.0 cm^2 were used as the counter electrode.

1.1.2.2. Experimental apparatus

The high-pressure experimental apparatus is shown in Fig. 4. Temperature variation of each run was confirmed to be less than 1.0 K. Maximum working temperature and maximum pressure were 424 K and 50 MPa, respectively. The reaction chamber was a stainless steel 316 vessel (PEEK coating on the inner wall) with a volume of 50 ml, kept in a temperature controlled air bath. There were holes at chamber cap for inflow and outflow of CO_2 and wiring. Through the holes, platinum wires inserted in PEEK tube were used to position the substrates and connected to a programmable power supply. A magnetic agitator with a cross-shaped magnetic-stirrer-bar was placed in the reaction chamber for mixing.

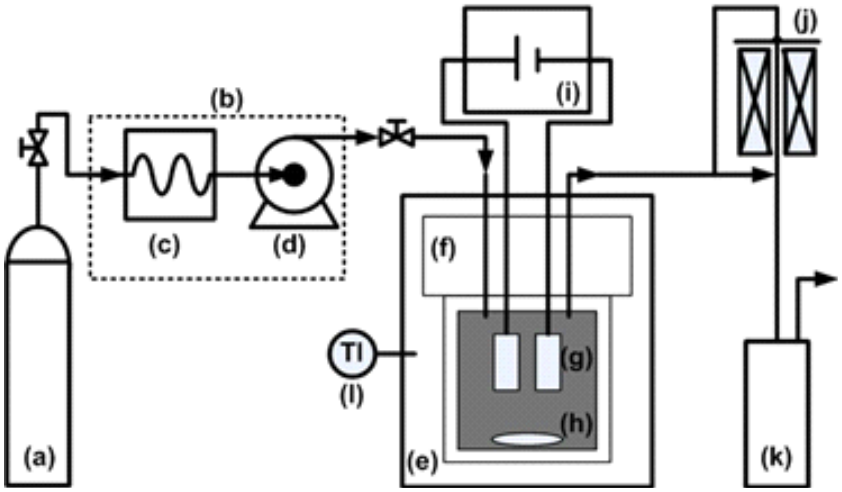

Figure 4. a) CO_2 gas tank, (b) liquidization unit, (c) liquidization pump, (d) high-pressure pump, (e) thermal bath, (f) reaction cell, with PEEK coating on the inner wall, (g) substrates, (h) stirrer, (i) programmable power supply, (j) back pressure regulator, (k) trap, (l) thermometer.

1.1.2.3. Electrodeposition

Cu plates were treated with 10 wt% degreasing solution and 10 wt% HCl solution for 1 min and 10 sec, respectively, prior to the reaction. Distance between the two substrates was 2.5 cm. Samples were electrodeposited at a constant temperature of 323 K with pressure vary-

ing from 9 to 18 MPa and current density from 0.01 to 0.20 A/cm^2. The deposition time was 30 min for all the samples. According to Faraday's Law, ca. 6 μm of Ni film would be electrodeposited if 100 % efficiency is achieved.

1.1.3. Effects of pressure

Physical properties of sc-CO_2, such as density, surface tension and viscosity, could be directly adjusted by pressure, which is also expected to affect physical properties of SCE. Pressure could also influence homogeneity of the emulsion, size of the DP, and population or concentration of the DP in the emulsion.

Circular marks/defects with diameter ranged from several to several tens of micrometers were found on surface of the Ni films electrodeposited at 9.0 MPa as shown in Fig. 5 (a) [22]. Size in diameter and total number of the circular marks decreased with increase in pressure. Overall surface uniformity of the Ni films improved significantly when pressure was rose to 18.0 MPa as shown in Fig. 5(c). Surface of the Ni films fabricated by EP-SCE was composed of nano-scaled particles as shown in Fig. 5, which was very different from electric field oriented conical-shape morphology of the Ni films electrodeposited without SCE at atmospheric pressure [23]. Average roughness (R_a)of the Ni films decreased from 19.22 to 12.10 nm as pressure was increased from 9.0 to 18.0 MPa, shown in Fig. 6. The relatively large standard deviation of R_a for the Ni films electrodeposited at 9.0 MPa was caused by the circular marks found on the surface. Standard deviation of R_a decreased significantly as surface uniformity of the Ni films improved with increase in pressure.

Chemical reaction in a reaction medium containing SCE is highly dependent on homogeneity of SCE [1]. High homogeneity of SCE is a prerequisite for fabrication of smooth film when applying SCE in electrodeposition. Homogeneity of SCE can be referred as stability, average size, and size distribution of the DP in the emulsion. SCE is a dynamically emulsified system; size of the DP could be continuously fluctuating in the emulsion. Stability of the DP is considered to be high when size fluctuation of the DP and tendency for phase separation to occur are both low. Quantitatively, the stability is high when interfacial tension between sc-CO_2 and the aqueous solution (γ) is low [24]. Growth in size of the DP is more likely to occur when γ is high, and continue growth in size of the DP would lead to phase separation. Creaming velocity (u_s) is another parameter that could be used to quantify stability of the DP [25]. Creaming is more likely to occur when u_s is high, and occurrence of creaming will lead to phase separation. u_s could be calculated using properties of the emulsion. Equation of u_s is shown in the following:

$$u_s = \frac{2r^2 \Delta\rho g}{9\mu_C} \tag{1}$$

where r is radius of the DP, $\Delta\rho$ is density difference between the DP and the CP, g is gravity, and μ_c is viscosity of the CP.

http://dx.doi.org/10.5772/54070

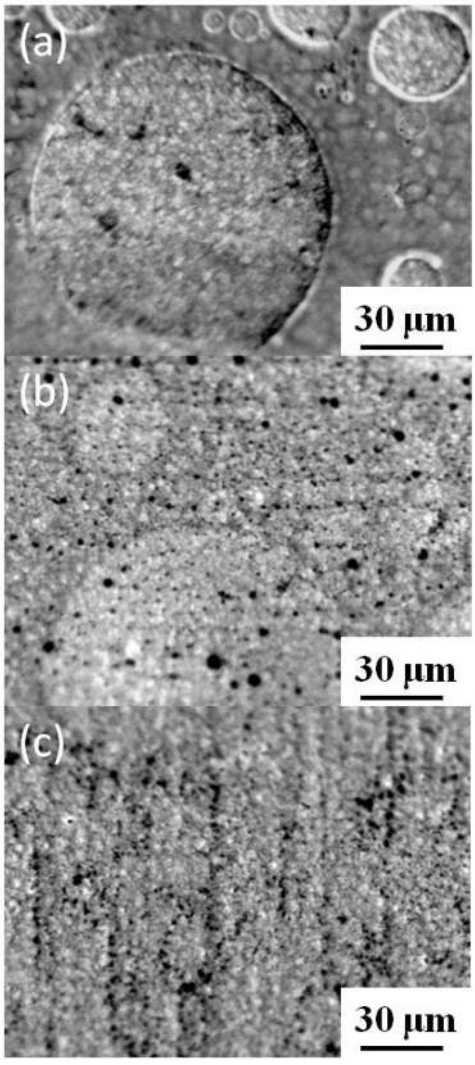

Figure 5. Ni films electroplated with SCE and pressure at (a) 9.0 MPa, (b) 12.0 MPa, and (c) 18.0 MPa.

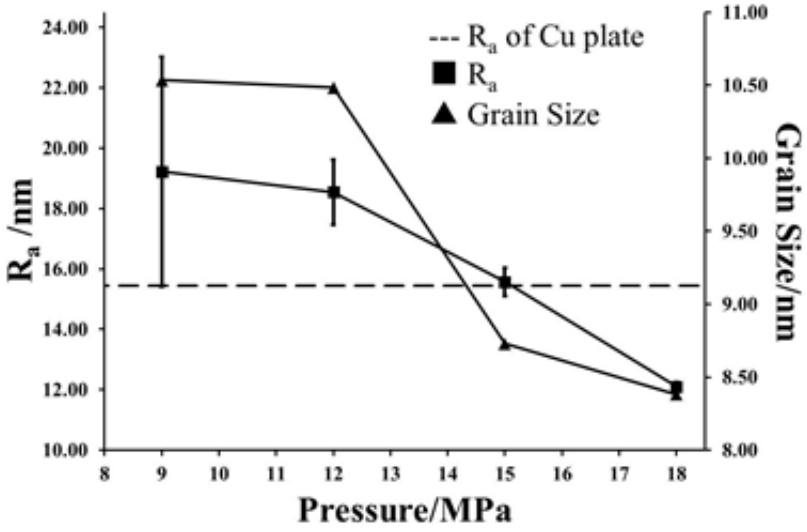

Figure 6. R_a and grain size of Ni films fabricated by EP-SCE at different pressure.

Both γ and u_s are highly related to density of CO_2 in SCE [24,25], and it has been reported that decrease in γ is observed when physical properties of the DP (mostly composed of CO_2) is adjusted to close to physical properties of the CP. For SCE, density and viscosity of the DP are both much lower than those of the CP, and both density and viscosity of the DP can be increased by increasing pressure. In addition, increase in density of the DP can also reduce $\Delta\rho$ in equation (1), which leads to decrease in u_s. Therefore, both γ and u_s are lowered and the stability is improved with increase in pressure. At 320K, density of sc-CO_2 increases from 320 to 770 kg/m^3 and viscosity from 24 to 65 μPa·s when pressure is increased from 9.0 to 18.0 MPa [1,26].

Major peak in XRD patterns of Ni films electrodeposited with SCE was (111) peak, which was caused by texture of the Cu plate, XRD patterns were shown in Fig. 7. Increase in pressure did not have significant influence on position of the (111) peak and relative intensity and position of both (200) and (220) peaks. Grain size calculated from Scherrer equation showed that grain refinement was observed with increase in pressure. Grain size decreased from 10.53 to 8.38 nm when pressure was increased from 9.0 to 18.0 MPa, shown in Fig. 6. Grain refinement is believed to be caused by the PPC when applying SCE in electrodeposition reaction, where adsorption and desorption of the DP from surface of the working electrode would cause a reaction-on and –off phenomenon, respectively.

More uniform size distribution of the DP can lead to more uniform on-time and off-time of PPC. Lee *et al*. and Dhanuka *et al*. both reported that average size of the DP reduced and the size distribution became more uniform with increase in pressure through dynamic light scattering measurement and direct SEM observation [12,24]. In addition, high pressure also favors monomer salvation over aggregates, which prevents aggregation of the DP.

http://dx.doi.org/10.5772/54070

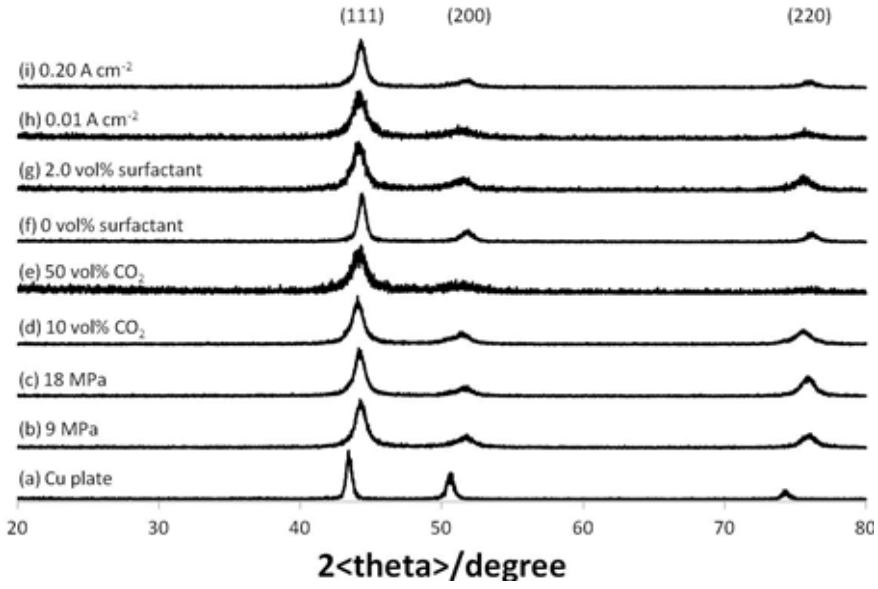

Figure 7. XRD patterns of the Cu plate and Ni films fabricated by EP-SCE with different conditions.

Decrease in size of the DP is expected to cause decrease in on-time of PPC. According to Einstein-Stokes equation, diffusion constant (D) of the DP is increased with a decrease in size of the DP. Einstein-Stokes equation is shown in the following:

$$D = \frac{k_B T}{6\pi\eta r} \tag{2}$$

where k_B is Boltzmann's constant, T is the absolute temperature, η is viscosity of the reaction medium, and r is the radius of the DP. Movement of the DP in SCE is faster with increase in D, and frequency of a particular region to have contact with the DP would be increased by faster mobility of the DP. This would be like decreasing on-time in pulse plating. Reduction in surface roughness and grain size of Ni film electrodeposited has been reported when on-time in pulse plating is decreased [27-29].

Desorption of H_2 gas bubbles from surface of cathode is also promoted with increase in pressure, because solubility of H_2 in sc-CO_2 is increased with increase in pressure. Combining the improved homogeneity, the PPC, the promoted H_2 gas bubbles desorption, R_a and grain size of the Ni film could be significantly reduced with increase in pressure for EP-SCE.

1.1.4. Effects of carbon dioxide volume fraction

Increasing volume fraction of CO_2 could increase total amount or concentration of the DP in SCE if enough surfactant is provided to maintain homogeneity of the DP. Desorption of H_2

gas bubbles from the surface of cathode is promoted when concentration of the DP is increased. Better desorption of H_2 gas bubbles then leads to improvement in uniformity of the surface and decrease in R_a of the Ni films electrodeposited. R_a decreased from 30.18 to 16.79 nm with CO_2 volume fraction increased from 10.0 to 50.0 vol%, shown in Fig. 8. Decrease in R_a is also contributed by decrease in on-time of the PPC, because frequency of adsorption and desorption between the DP and the working electrode is increased with increase in concentration of the DP. This decrease in on-time also leads to decrease in grain size of the Ni films electrodeposited. Grain size was found to reduce from 9.41 to 8.02 nm when CO_2 volume fraction was increased from 10.0 to 50.0 vol%, shown in Fig. 8.

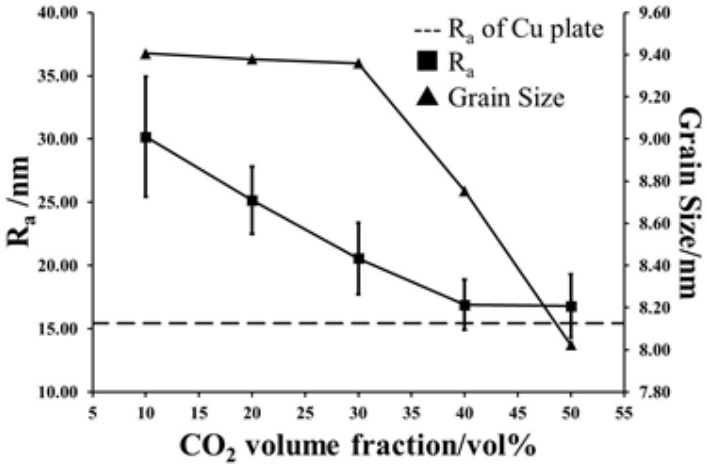

Figure 8. R_a and grain size of Ni films fabricated by EP-SCE with different CO_2 volume fraction.

Defects were found on the surface for Ni films electrodeposited with CO_2 volume fraction higher than 50.0 vol%. The defects were caused by adsorption of the DP on the surface of cathode when homogeneity of the emulsion is too low. Increase in size and size distribution of the DP occur when CO_2 volume fraction is increased while temperature, pressure, and volume fraction of the surfactant remain fixed in the system [12]. Growth in size of the DP is an indication of poor homogeneity, and continues increasing volume fraction of CO_2 in the system would eventually lead to phase separation. Some portion at the upper part of the Cu plate was found to be not electrodeposited with Ni when volume fraction of CO_2 was increased to 60.0 vol%. When 60.0 vol% of CO_2 was used, ca. 13% of the surface was found to be not covered by electrodeposited Ni, the value increased to 26% and 50% when CO_2 volume fraction was increased to 70.0 and 80.0 vol%, respectively.

1.1.5. Effects of the surfactant volume fraction

Usage of the surfactant in the system allows formation of the DP. Uniformity of the surface improved significantly when 0.1 vol% of the surfactant was used when comparing with the

http://dx.doi.org/10.5772/54070

Ni film electrodeposited without addition of the surfactant. R_a of the Ni films decreased dramatically from 89.67 to 18.93 nm as volume fraction of the surfactant increased from 0 to 0.1 vol% as shown in Fig. 9, and R_a was 16.90 and 17.04 nm when 1.0 and 2.0 vol% of the surfactant, respectively, was used. Increasing volume fraction of the surfactant is expected to cause reduction in size of the DP, because γ is reduced with increase in volume fraction of the surfactant [24], therefore, on-time of the PPC is decreased and causes grain size to decrease. Grain size decreased from 15.23 to 8.81 nm for surfactant volume fraction from 0 to 2.0 vol%., shown in Fig. 9. Volume fraction of CO_2 was fixed for the samples prepared with various volume fraction of the surfactant. Both R_a and grain size of the Ni films did not decrease much from 1.0 to 2.0 vol% of the surfactant used. This indicates concentration of the surfactant is close to saturation at ca. 1.0 vol%.

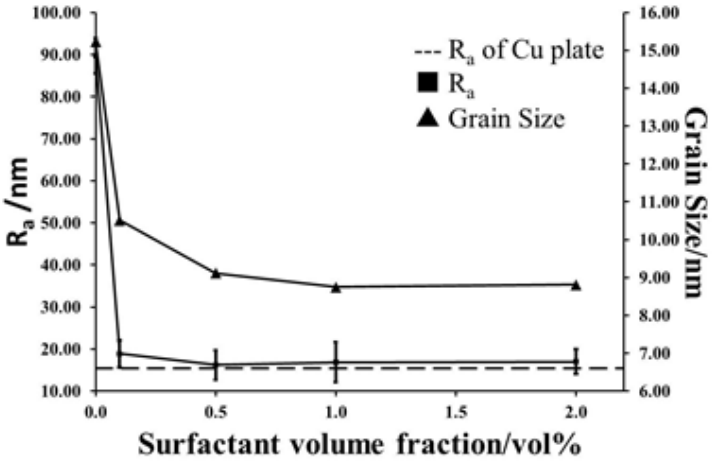

Figure 9. R_a and grain size of Ni films fabricated by EP-SCE with different surfactant volume fraction.

1.2. Periodic-plating-characteristic

Direct observation of PPC is extremely difficult because of the electrolyte is actually composed of heterogeneous emulsion and the high pressure. Indirect evidence of PPC was reported in Rahman et al.'s work [30] as shown in Fig. 10. The porous structures were expected to be caused by adsorption of the dispersed phase (DP), since electrodeposition reaction would be restrained in the region on the working electrode where it is covered by the DP. However, direct observation of PPC in EP-SCE is still required, but direct observation is extremely difficult because of the high pressure environment and heterogeneous emulsified electrolyte. In addition, size of the DP or the micelle is usually in the micro- or even nanoscale range [31,32]. This increases the difficulty for observation of the periodically reaction-on and –off phenomenon directly.

The periodically adsorption and desorption of the DP is expected to cause a difference in the actual surface area available for the electrochemical reaction. Therefore, a fluctuation in the potential response would be expected if a constant current is applied to the system if the difference in the actual surface area available is significant enough. Based on these assumptions, an electroanalytical method, chronopotentiometry (CP), and a modified working electrode are used to directly observed the PPC.

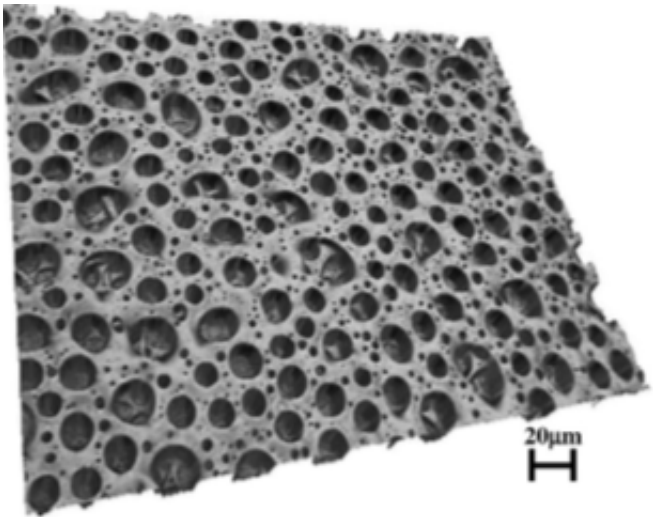

Figure 10. Porous Ni film fabricated by Ni ESCE.

In order to magnify the fluctuation in the potential response obtained from CP, small contact area between the working electrode and the electrolyte is used as shown in Fig. 11. Area of the working electrode having contact with the electrolyte would be only the tip of the Ø0.5 mm Cu wire, and the area is 0.196 mm^2.

Figure 11. Working electrode used for direct observation of PPC.

http://dx.doi.org/10.5772/54070

Fluctuation in potential response was not observed for conventional electrodeposition as shown in Fig. 12(a). When EP-SCE was used, fluctuation in the potential response was observed as shown in Fig. 12(b). The fluctuation indicates the change on the surface condition of the working electrode, and this is most likely to be caused by adsorption and desorption of the DP. The surfactant used for form SCE was added to the Ni electrolyte without using the sc-CO_2 to confirm the cause of the fluctuation, and the no fluctuation was observed as shown in Fig. 12(c). This result showed the fluctuation was not caused solely by the surfactant. Hence, we could confirm that the fluctuation observed in Fig. 12(b) is a direct observation of PPC.

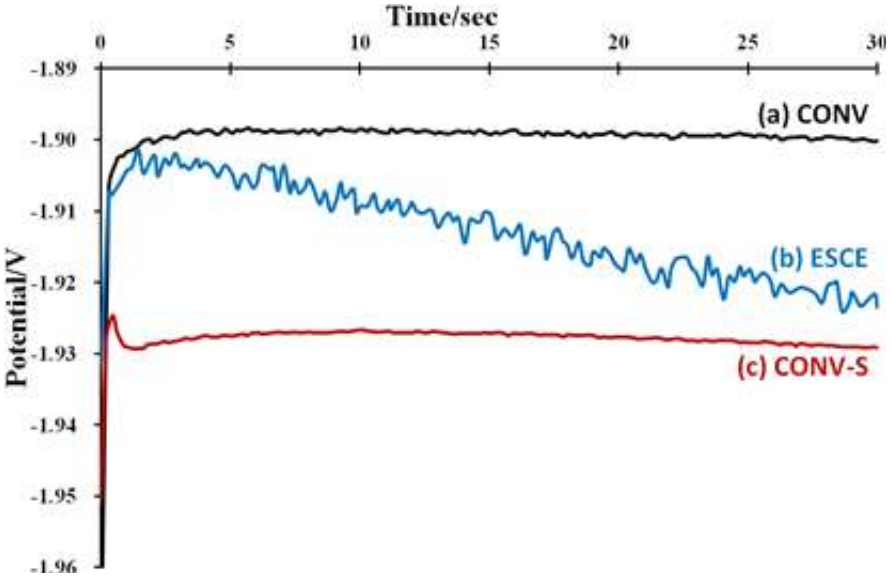

Figure 12. Working electrode used for direct observation of PPC.(a) Conventional electrodeposition, (b) ESCE, and (c) conventional electrodeposition with addition of the surfactant. Current density applied was 0.020 A/cm^2.

1.3. Application of EP-SCE

In fabrication of micro-structures used for Micro-Electro-Mechanical systems, electrodeposition with a template made up of photoresist patterns on top of a conductive substrate is often used as shown in Fig. 13. The photoresist patterns are used to confine dimensions of the structures electrodeposited on the conductive substrate. However, transport of H_2 gas bubbles away from the reaction site is less efficient at the bottom/holes of the photoresist patterns, and H_2 gas bubbles remained at the bottom of the photoresist patterns would cause formation of defects in the micro-structures fabricated. There are several methods to eliminate the problems caused by evolution of H_2. The most often applied method is reducing the evolution rate of H_2 using a lower current density, but growth rate of the micro-structures is

also decreased with low current density. Removal of the H_2 gas bubbles from the reaction site is known to be improved by application of SCE. In this way, high current density and high growth rate of the micro-structures could be assured by application of EP-SCE.

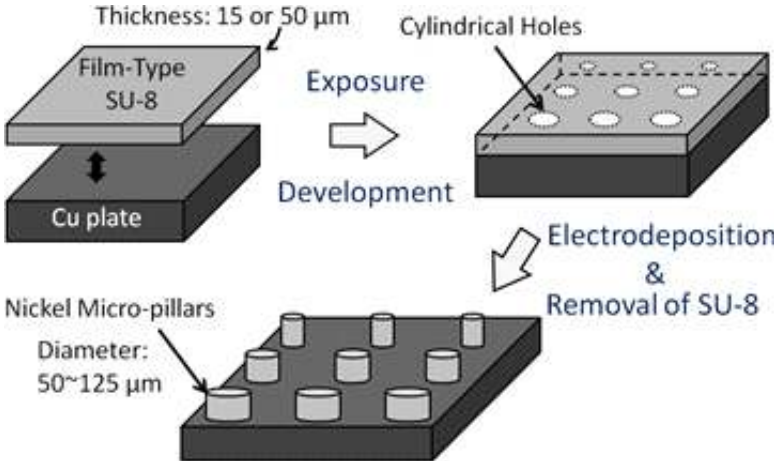

Figure 13. Procedures for fabrication micro-structures.

Ni micro-structures fabrication by conventional electrodeposition with a current density are defective, shown in Fig. 14(a) and (b). These defects were caused by H_2 gas bubbles remained inside the photoresist patterns. On the other hand, when EP-SCE was applied, defect-free Ni micro-structures could be obtained even when a high current density was used, shown in Fig. 14(c), and the average growth rate of the Ni micro-structures was about 5.1 µm/min.

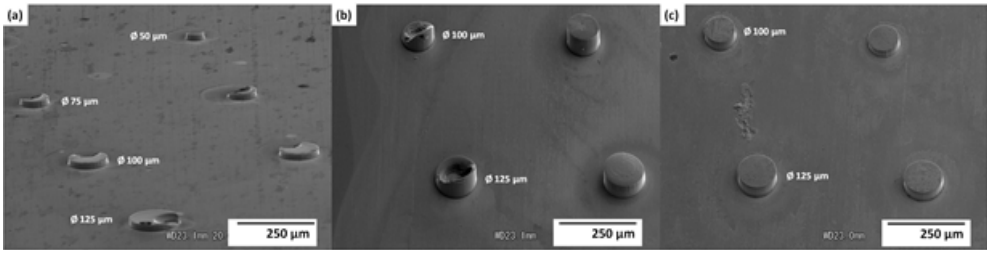

Figure 14. Ni micro-structures fabricated by (a) conventional electrodepositon at 0.100 A/cm_2 for 3 min, (b) conventional electrodepositon and (c) ESCE at 0.100 A/cm2 for 5 min.

http://dx.doi.org/10.5772/54070

1.4. Conclusion

Physical properties of SCE are found to be affected by pressure, volume fraction of CO_2 and the surfactant. Improvement in homogeneity of SCE is achieved by increasing pressure. Therefore, size and size distribution of the DP are reduced as shown in Fig. 15(a) and (c). Since volume fraction of CO_2 in the system is fixed, therefore, reduction in the size would lead to increase in concentration of the DP, and this is expected to cause decrease in on-time of PPC and decrease in R_a and grain size. Increase in volume fraction of CO_2 leads to increase in concentration of the DP, and the size and size distribution would remain small if enough surfactant is present in the system, shown in Fig. 15(b) to (c). Growth in size of the DP would occur if insufficient amount of the surfactant is present to stabilize CO_2 introduced into the system, and continue growth in size of the DP would lead to phase separation as shown in Fig. 15(d). Phase separation could be prevented by increasing pressure or volume fraction of the surfactant, which lowers γ and u_s. Improvement in stability and reduction in size and size distribution of the DP are achieved with increase in volume fraction of the surfactant as shown in Fig. 15(e) and (c). This is why both R_a and grain size is lowered with increase in volume fraction of the surfactant used. We also studied and proposed a mechanism called periodic-plating-characteristic (PPC) to be the main cause for the effects observed in the metal films fabricated by EP-SCE. Moreover, we directly observed PPC by an electroanalytical method, chronopotentiometry (CP), and a modified working electrode. On these experimental results, we applied EP-SCE on fabrication of microstructure and succeeded.

2. Crystal growth by electroless Ni-P plating using supercritical carbon dioxide emulsion

2.1. Electroless plating in a supercritical CO_2 emulsion (ELP-SCE)

2.1.1. Introduction

Electroless plating (ELP) has a low processing temperature, a high metal-ion transportation density, the ability to deposit on electrically nonconductive materials, a more uniform thickness for products of any shape, and a simple deposition mechanism.[33,34] A wet process such as ELP can serve as a superior alternative for a three-dimensional (3D) integration technology. The disadvantages of ELP are the high viscosity of the solution and anomalous growths in the plating film caused by the pretreatment condition. These disadvantages have interfered with the formation of microstructures for electronic devices and MEMS.

The key requirement for forming a uniform, conformal thin film over a complex 3D micro/nanostructure will be to improve the transport properties. To this end, we propose a technique based on the criteria mentioned above. Specifically, we proposed an ELP method using dense carbon dioxide (CO_2) beyond the critical point as a solvent. The changeable density of dense CO_2 enables excellent control of the intermolecular interactions, and the high density

and diffusivity of the material assure that the plating films can form over nanoscale areas with outstanding reliability. Supercritical carbon dioxide (sc–CO_2), however, has been found to be unsuitable as a medium for plating reactions. Metal salts are generally soluble in water, but water and CO_2 tend to mix poorly. The problem can be solved by emulsifying sc–CO_2 and a plating solution, then adding a nonionic surfactant.[13] The ELP technique we propose in this study uses a dense CO_2 beyond the critical point. The ELP reaction in Electroless Plating in a Supercritical CO_2 Emulsion (ELP-SCE) [35] takes place in an emulsion containing dense CO_2. We discuss the surface morphology of the film plated by ELP-SCE, which turns out to have various advantages over the surface morphology of film plated by conventional ELP.

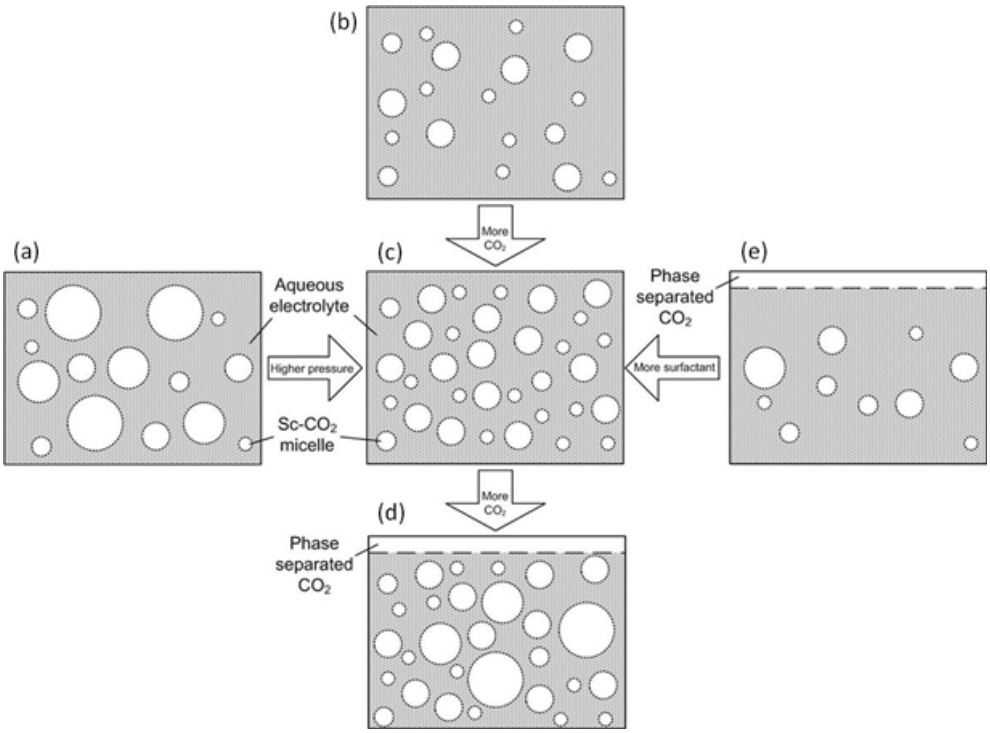

Figure 15. Illustration of conditions of the DP in SCE: (a) at relatively low pressure, (b) at relatively low CO_2 volume fraction, (c) at relatively high pressure, medium CO_2 volume fraction, and high surfactant volume fraction, (d) at relatively high CO_2 volume fraction, and (e) at relatively low surfactant volume fraction. .

http://dx.doi.org/10.5772/54070

	Reducing Agent						
Metal	$H_2PO_2^-$	N_2H_4	CH_2O	BH_4	RBH_3	Me ions	Others
Ni	Ni-P	Ni		Ni-B	Ni-B		
Co	Co-P	Co	Co	Co-B	Co-B		
Fe				Fe-B			
Cu	Cu	Cu	Cu	Cu	Cu	Cu	
Ag		Ag	Ag	Ag	Ag	Ag	Ag
Au		Au	Au	Au	Au		Au
Pd	Pd-P	Pd	Pd	Pd-B	Pd-B		
Rh		Rh					Rh
Ru				Ru			
Pt		Pt		Pt			Pt
Sn						Sn	
Pb			Pb				

Table 2. Coating Obtained by Electroless Plating

2.1.2. Electroless plating reaction and experimental method

The ELP methods currently known can be used to deposit 12 different metals (Table 2). [34] Decomposition products (phosphorous and boron) in the reducing agent precipitate as the metal deposits, leaving films of the respective alloys. Two or more metals can be deposited at once without much difficulty. ELP methods are used for the deposition of more than 50 alloys of different qualitative compositions, mostly based on nickel, cobalt, and copper. For this study we selected an electroless nickel-phosphorus (Ni-P) plating process. The most widespread type of Ni-P plating uses hypophosphite as the reducing agent.[33,34][4] Three major properties of electroless Ni-P, namely, its hardness, wear resistance, and corrosion resistance, have led to its technical application in many industries, from electronics, automaking, aerospace, and machinery to oil and gas production, power generation, printing, and textiles. The process is generally applied with a stable, acidic Ni-P plating solution, as contact with CO_2 acidifies water due to the formation and dissociation of carbonic acid.

2.1.2.1. Materials

CO_2 with a minimum purity of 99.99% was purchased from Nippon Tansan Co., Ltd. The experiments were performed with a nonionic surfactant polyoxyethylene lauryl ether ($C_{12}H_{25}(OCH_2CH_2)_{15}OH$) supplied by Toshin Yuka Kogyo. The electroless Ni–P plating solution had a chemical composition of nickel chloride (9%), sodium hypophosphite (12%), complexing agent (12%), and ion-exchanged water (67%) (Okuno Chemical Industries Co., Ltd.). The substrate was a 99.99% pure film of copper measuring 10×20 mm (Mitsubishi Shindoh Co., Ltd). The substrate was washed with acetone and rinsed in deionized water before each reaction. The grease was removed from the sample by successive dipping in a 10 wt % solution of NaOH and a 10 wt % solution HCl followed by rinsing in deionized water. The sample was added to an activator solution consisting of hydrogen chloride (18%), palladium chloride (0.04%), and ion-exchanged water (81.96%) (Okuno Chemical Industries Co., Ltd.)

at 303 K, then rinsed in deionized water. This pretreatment was applied to all copper substrates regardless of the condition of the ELP.

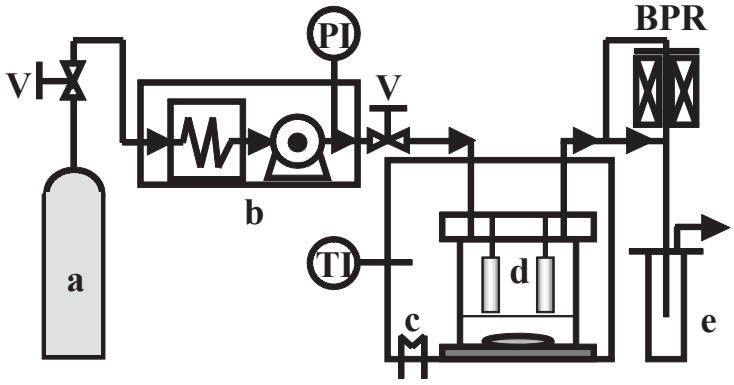

Figure 16. Experimental apparatus used for batch reaction in our electroless plating experiments beyond the critical point of CO_2; (a) CO_2 cylinder; (b) cooler and high pressure pump; (c) temperature controlled air bath; (d) reactor with magnetic stirrer; and (e) trap; BPR: back-pressure regulator; PI: pressure indicator; TI: temperature indicator; V: valves.

2.1.2.2. Experimental apparatus and procedure

Fig. 16 shows the high-pressure experimental apparatus (Japan Spectra Company) used for the ELP.[35] The temperature variation of each run was confirmed to be less than 1.0 K. The maximum working temperature and the maximum pressure were 424 K and 50 MPa, respectively. The reactor was a stainless steel 316 vessel with an internal volume of 50 mL, kept in a temperature-controlled air bath. A magnetic agitator with a cross-magnetic stirrer bar was placed within the reactor and the activated substrate was attached to the reactor with stainless wires. A plating reaction within a reactor starts only upon contact between the substrate and plating solution. As such, the substrate position in a reactor affects both the reproducibility and surface morphology of the ELP film. Yan et al. demonstrated the dispersion behaviors of a ternary system composed of dense CO_2, an electroplating (EP) solution, and a surfactant.[14] Their experiment was performed in a high-pressure view cell with an internal volume of 45 mL. In the absence of stirring, two separated phases, namely, a transparent upper CO_2 phase and a clear green lower phase (the nickel EP solution) were observed at 323 K and 10 MPa. The ternary system with the CO_2 volume fraction of 0.2 was stirred at 400 rpm. The CO_2 dispersed into the plating solution with stirring, and the light scattering from the small CO_2 drops in the solution increased the turbidity of the system. In our experiment, before the ELP reaction, the electroless Ni–P plating solution (30 mL) and surfactant (surfactant concentration: 1.0 wt % to the ELP solution) were placed in the reactor at atmospheric pressure. Next, liquid CO_2 was pumped into the cell by a high performance liquid chromatography (HPLC) pump until a predetermined pressure was reached. The ELP reaction was performed at a temperature of 353 K and a pressure of 15 MPa in a constantly

http://dx.doi.org/10.5772/54070

agitating ternary system stirred at a speed of 500 rpm. The reaction commenced from the start of agitation. In the Results and Discussion of this chapter we describe the properties of the plated film fabricated by ELP-SCE in comparison with those of film fabricated by conventional ELP. The conventional method was performed under the following experimental conditions: 353 K, atmospheric pressure, a plating solution with a chemical composition identical that used in ELP-SCE, constant stirring at a speed of 50 rpm.

2.1.2.3. Analysis

An optical microscope (Digital Microscope VHX-500, Keyence. Co., Ltd.) and scanning electron microscope (FE-SEM, S-4500, Hitachi High-Technologies Co., Ltd.) were used to study the surfaces of the plated Ni–P films. A surface texture measuring instrument (Surfcom 480A, Tokyo Seimitsu Co., Ltd.) with a diamond-tipped detector (2 μm tip radius) was used to measure the average surface roughness (*Ra*) to a minimum height resolution of 1 nm (height measurement range: 80 μm). The average *Ra* was calculated from measurements at five points or more. The film thickness was measured directly from a cross-sectional scanning electron microscopy (SEM) image of a plated Ni–P film fabricated by a focused ion beam system (FB-2100, Hitachi High-Technologies Co., Ltd.). The phosphorus composition of the fabricated film was measured by an FE-SEM (S-4300SE, Hitachi High-Technologies Co. Ltd.) equipped for energy-dispersive X-ray spectroscopy (EDX). An accelerating voltage of 20 kV with a collecting time of more than 300 s was applied. X-ray diffraction (XRD) analysis (2θ-ω scans) was performed at room temperature (RT, 298 K) using a PANalytical X'pert Pro Galaxy system equipped with an X'celerator module. The X-ray source was CuKα, and the tube voltage and current were 45 kV and 40 mA, respectively.

2.1.3. Electroless Ni-P plating in an emulsion of supercritical CO_2

Fig. 17 shows optical microscope images of a copper substrate and Ni-P films plated over the substrate by ELP-SCE at 15 MPa and 6 MPa. Polishing trace was observable on the copper substrate before pretreatment. The film plated at 15 MPa was uniformly bright and covered both the front and back of the substrate (Fig. 17 (b)). The uniform brightness and coverage were attributable to the exact position of the substrate and the uniformity of the emulsion. The formation of emulsion was unstable in the film plated at 6 MPa, beyond the critical point, so the film was thin and even unformed in portions (Fig. 17 (c)). The surface roughness (*Ra*) of the plating films was 0.030 μm at 15 MPa and 0.059 μm at 6 MPa.

If CO_2 exceeds a critical point, the density will rise rapidly. While the CO_2 density at 323 K and 6 MPa is only 0.1 kg L^{-1}, it reaches 0.7 kg L^{-1} at the higher pressure of 15 MPa.[8] Moreover, Sone et al. reported that in a ternary system of water, surfactant, and CO_2, the CO_2 formation in the water emulsion by the surfactant is affected not only by the temperature and pressure, but also agitation.[4] They also found, in a similar experiment, that no emulsion was formed below the critical point. With ELP-SCE, a stable emulsion forms when the CO_2 density approaches the liquid phase, and a uniform plating film can be deposited.

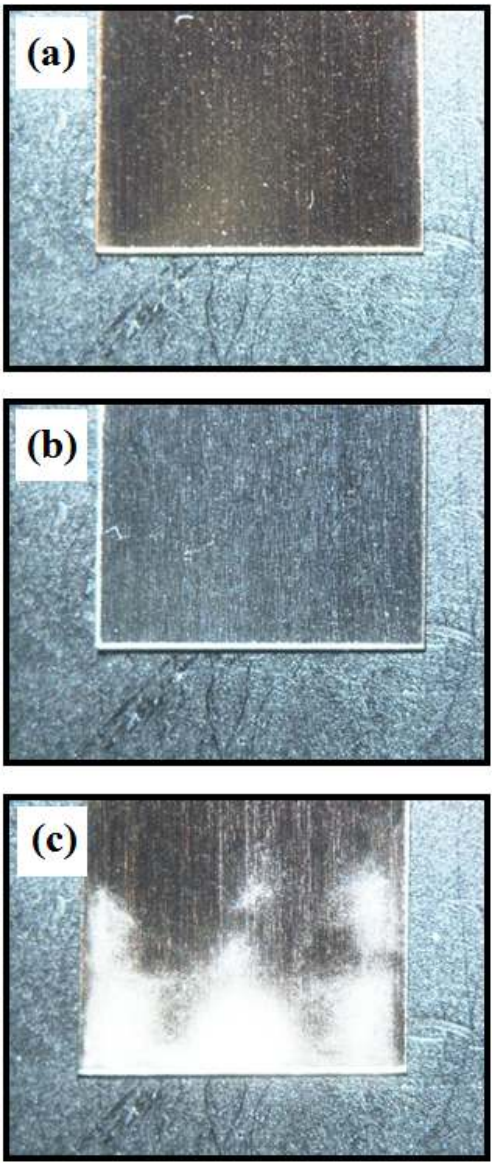

Figure 17. Optical microscopy images of (a) pure Cu substrate and Ni–P films plated from ELP-SCE at 353 K for 60 min (b) at 15 MPa and (c) at 6 MPa.

http://dx.doi.org/10.5772/54070

According to an as-deposited coating surface composition analysis by EDX, the Ni-P film formed by ELP-SCE was composed of 20 wt % phosphorus. When the phosphorus content increases, the microstructure of an electroless Ni-P deposit changes from a mixture of amorphous and nanocrystalline phases to a fully amorphous phase.[36] The structure of our Ni-P film was confirmed to be amorphous by XRD. Amorphous profiles with a wide angular range of 40-45° (2θ) appear nearby a 2θ position corresponding to the Ni {111} plane. The copper substrate underneath was responsible for the Cu diffraction peaks in the profiles of the Ni-P film formed by ELP-SCE. The peaks appear because the coated-deposit was too thin (1.0 μm less) to totally absorb the penetration of the X-ray beam (Fig. 18).

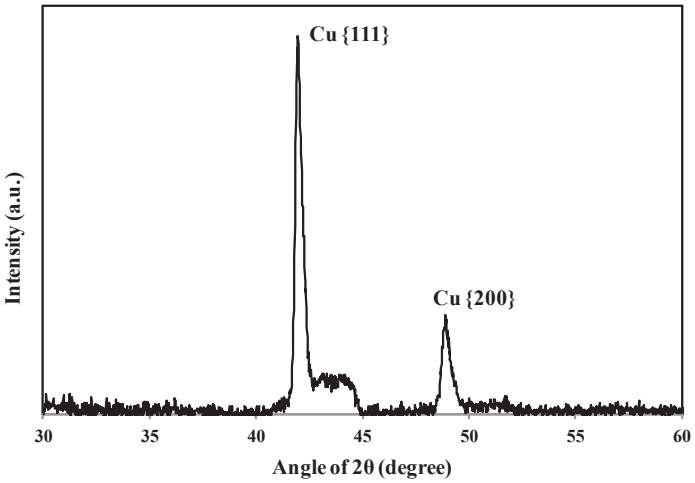

Figure 18. XRD spectrum of Ni-P film plated from ELP-SCE at 353K and 15 MPa for 180 min.

2.1.4. Surface morphology of Ni-P film by conventional ELP and ELP-SCE

We used an optical microscope to observe the surface features of a Ni–P film formed by conventional ELP, another Ni–P film formed by ELP-SCE, and a pure copper substrate (Fig. 19). The only clear difference in defects between the two Ni–P films was a polishing trace on the copper substrate. As is widely known, thin films fabricated by ELP have smaller pinholes and cracks than those fabricated by EP.

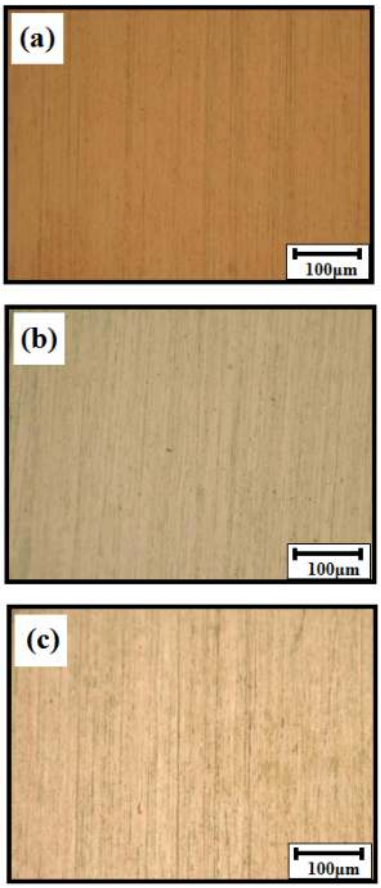

Figure 19. Optical microscopy images of Ni–P films plated from (a) ELP-SCE at 353 K and 15 MPa for 180 min, (b) conventional ELP at 353 K and atmospheric pressure for 2 min, and (c) pure copper substrate.

SEM observations reveal clear differences between the surface morphologies of the Ni–P films and the substrate activated by catalytic Pd, as shown in Fig. 20. The thickness of the Ni–P film fabricated by conventional ELP was 0.3 μm, while that fabricated by ELP-SCE was 0.8 μm. Nodules were observed on the Ni–P film fabricated by conventional ELP in the early stage of the reaction, as shown in Fig. 20 (b). This nodule formation was the result of concentrated nickel reactions over a localized area on Pd nucleus on the surface of the substrate as shown in Fig. 20(c). Earlier reports also have confirmed that the nickel nucleus appears and grows on the Pd nucleus on the surface of the substrate.[37-39] These nodules become a serious problem when they form in films fabricated by ELP on fine electronic devices and MEMS. Meanwhile, the thin film fabricated by ELP-SCE was free from nodules and pinholes, but its thickness was still more than double that of the thin film fabricated by conven-

http://dx.doi.org/10.5772/54070

tional ELP. The only particles observed were extremely fine, with diameters of several tens of nm or less (Fig. 20 (a)).

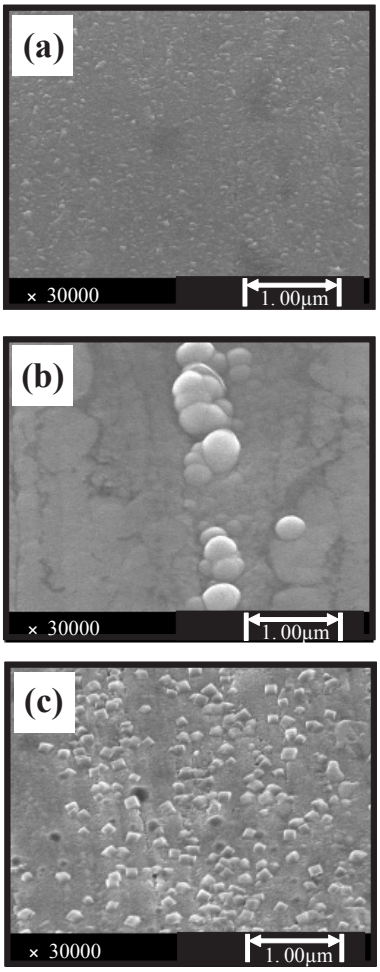

Figure 20. SEM images of Ni–P films plated from (a) ELP-SCE at 353 K and 15 MPa for 180 min, (b) conventional ELP at 353 K and atmospheric pressure for 2 min, and (c) substrate activated by catalytic Pd.

Fig. 21 shows how variations in the reaction time influence the surface features of the Ni–P films formed by conventional ELP and by ELP-SCE. The plating films formed by conventional plating for 5.0 and 30 min had thicknesses of 0.8 and 4.9 μm, respectively. The plating films formed by ELP-SCE for 360 and 540 min had thicknesses of 0.9 and 1.0 μm, respectively. The SEM images reveal nodules on all of the surfaces of the Ni–P films fabricated by conventional ELP (Fig. 20 (b), 21 (c), and 21 (d)). The images also show that the nodules

increased, both in size (from several hundred nm to over several μm) and in number, as the reaction time increased.

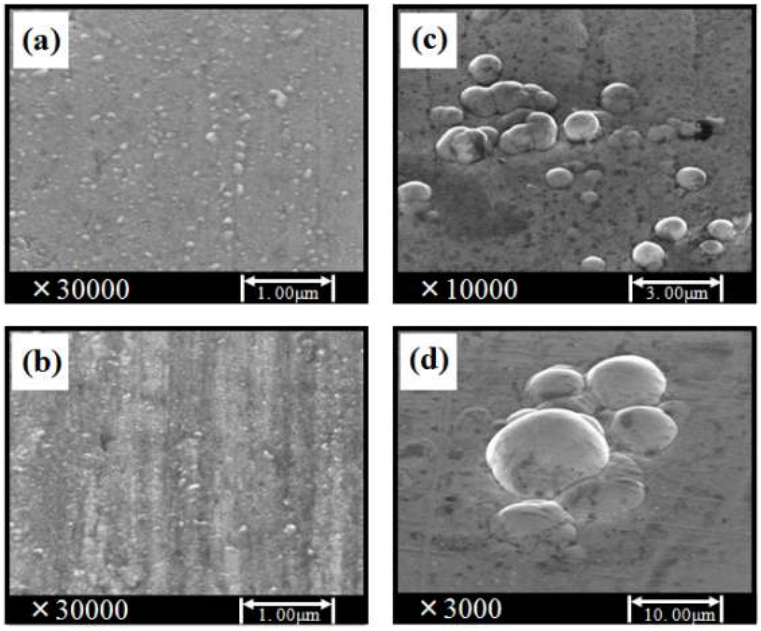

Figure 21. SEM images of Ni–P films plated from ELP-SCE at 353 K and 15 MPa for reaction times of (a) 360 min and (b) 540 min, and conventional ELP at 353 K and atmospheric pressure for (c) 5 min and (d) 30 min.

Meanwhile, the Ni–P film fabricated by ELP-SCE was free of nodules (Fig. 20 (a)) and had an extremely uniform surface (Figs. 21 (a) and (b)). These results differed considerably from the changes in the surface features of conventional ELP films brought about by adjustments in the reaction time and the processing methods for the substrate activation by Pd. [37-39] We also found that our ELP technique could fabricate superb, highly uniform plated films even when the substrate pretreatment, reaction temperature, and chemical composition of the electroless Ni–P plating solution were all identical to those use d in conventional ELP. On this basis, we surmise that our ELP technique may be effective in suppressing the growth of nodules.

Fig. 22 shows the roughness curves on the surfaces of the Ni–P films formed by ELP-SCE, by conventional ELP, and by surface activation of the substrate. The evaluation length of the surface roughness measurement was 1.250 mm. The activated substrate had an *Ra* of 0.040 μm. The conventional ELP had an *Ra* of 0.048 μm and a rougher surface than the activated substrate. Previous reports have shown how activation processing changes the surface morphologies and deposition behaviors of electroless Ni–P films. [37-39] Meanwhile, ELP-SCE formed a film with improved smoothness (*Ra* of 0.030 μm)

http://dx.doi.org/10.5772/54070

under the same activation processing conditions used for conventional ELP. We also found that the film thickness conferred a strong influence on the surface roughness. The thin film formed by ELP-SCE was very smooth, though it was still more than twice as thick as the film fabricated by conventional ELP. These results demonstrate that ELP-SCE suppressed the deposition reaction of the locally concentrated nickel. We can also see, in Fig. 20 and Fig. 21, that no nodules were formed.

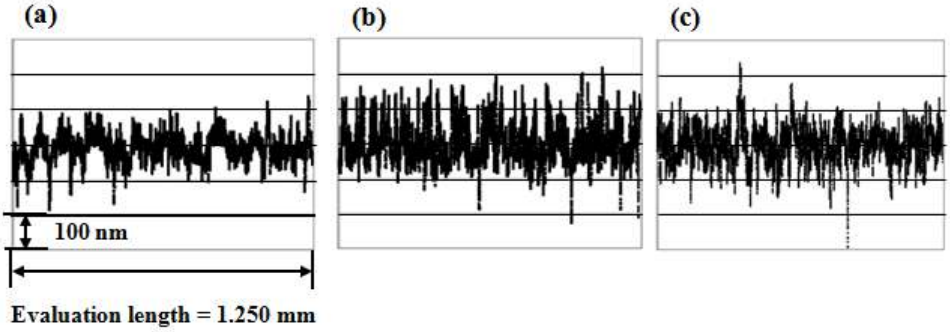

Figure 22. Roughness curves of the surfaces of Ni–P films plated by (a) ELP-SCE at 353 K and 15 MPa for 180 min, (b) conventional ELP at 353 K and atmospheric pressure for 2 min, and (c) substrate activated by catalytic Pd.

The conventional ELP as performed at 353 K and atmospheric pressure. ELP-SCE was performed at 353 K and 15 MPa. Fig. 23 shows the relationship between the surface roughness and reaction time. The surface of the Ni–P film fabricated by the conventional ELP roughened as the reaction time increased. The roughness of the Ni–P film formed by ELP-SCE, meanwhile, showed no dependence on the reaction time. Nodules appeared on the surfaces of the Ni–P films fabricated by conventional ELP at all reaction times, and the nodules grew as the reaction times increased. No nodules were observed on the surfaces of any of the Ni–P films fabricated by ELP-SCE, even at the maximum reaction times. The aforementioned results confirm that the excellent smoothness of ELP-SCE film mitigated the influence of the substrate pretreatment and was independent of the reaction time. Fig. 20, meanwhile, shows a suppression of the growth of the nodules generated by conventional ELP.

ELP-SCE produced a thin film with high smoothness and outstanding uniformity. The Ni–P film fabricated by conventional ELP with a reaction time of 5 min had a thickness of 0.8 μm, or about the same thickness as ELP-SCe film fabricated with a reaction time of 180 min. The *Ra* of the ELP-SCE film was 0.03 μm, while that of the conventional ELP film was 0.06 μm.

ELP films are generally smoother than EP films and have fewer defects.[40] Even with ELP, however, defects such as microscopic nodules, pits, and pinholes are difficult to suppress. [41-43] Although suppression of a through-hole like a pinhole need a thick film, more nodules form in a thicker film. Nodules also easily form when the underlayer has projecting parts, foreign objects, and nuclear growth sites. Conventional suppression of nodule method

prepares the smoothness and cleanness of an underlayer, while nonlinear diffusion adds reactive species that interfere with film growth over the projecting parts of a plating film (see Fig. 24).[44] Further, the pulse electroplating controls the thickness of a diffusion layer and is available to suppress nodule growth. [45]

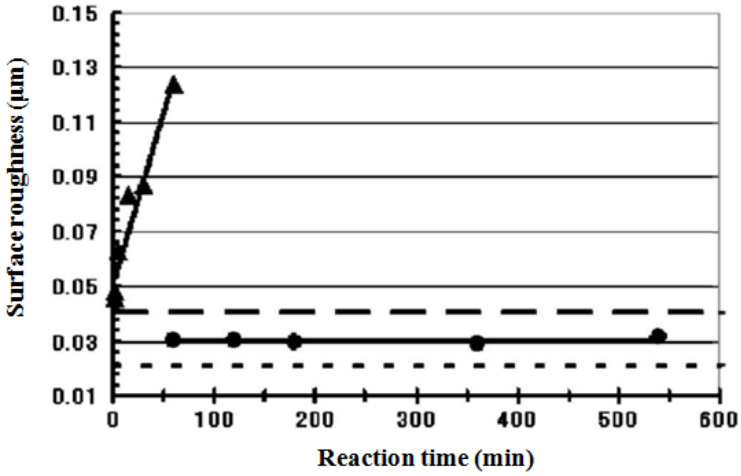

Figure 23. Relationship between Ra and reaction time. Ra of the Ni–P film made by ELP-SCE and by conventional ELP are plotted as circles and triangles, respectively. The dotted line shows Ra of the activated substrate and the fine dotted line shows the surface roughness of the pure Cu substrate.

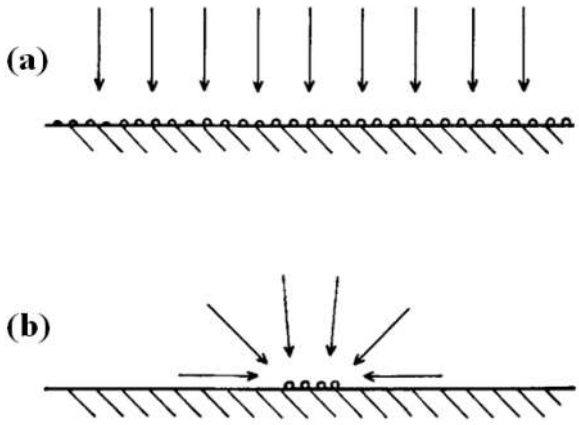

Figure 24. a) Linear O_2 diffusion to a large activated area. (b) Linear and nonlinear O_2 diffusion to a small pattern of nuclei.[15]

http://dx.doi.org/10.5772/54070

ELP-SCE formed very smooth thin films whose thicknesses suppressed both nodules and pinholes without exceeding even 1 μm. The pH, reaction temperature, pretreatment, stirring speed, additive, and reactive species concentration in the plating solution all influence the deposition behavior of the ELP film. Yet in our current work we used the same plating solution, reaction temperature, and pretreatment for both ELP-SCE and conventional ELP.

The Ni–P film plated by ELP-SCE was free of pits and pinholes because the hydrogen bubbles produced by the electrolysis of the water were dissolved in the dispersed sc–CO_2 phase of the emulsion.[13] Moreover, ELP-SCE plates the film under high pressure. High-pressure plating failed to deliver good results because hydrogen bubbles were less buoyant in the high-pressure system than at atmospheric pressure. Hence, the larger bubbles prevent the metal from covering the substrate. This, a characteristic effect of plating techniques that use sc-CO_2 emulsion, suppresses the formation of pits or pinholes via the mechanism shown in Fig. 25.

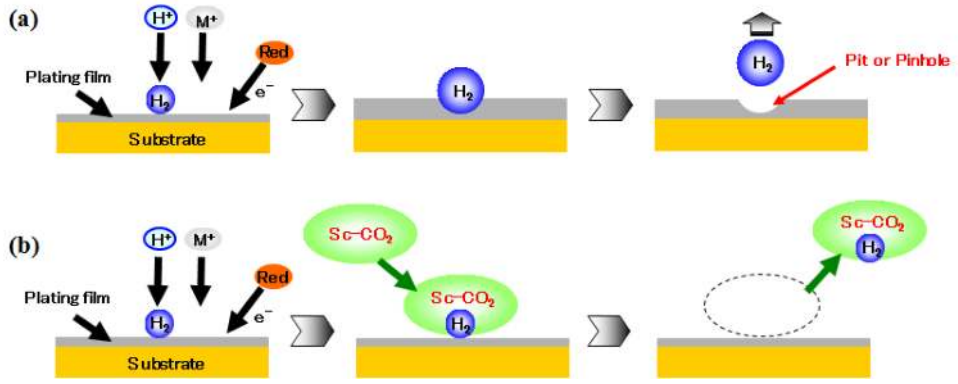

Figure 25. a) Pinhole formation in conventional electroless plating. (b) Suppressed pinhole formation in ELP-SCE. M: metal, Red: reducing agent, and sc-CO_2: supercritical carbon dioxide.

The best feature of ELP-SCE is its ability to suppress nodules and other abnormal growths formed by the plating reaction. The electroless metal deposition occurs by repeated 3D nucleation at catalytic sites on the substrate.[46] In 3D growth of the deposited Ni under a low-nucleation-density condition, the deposited Ni grows and the surface roughness increases. Further, an activation processing technique with Pd catalyst can be used to influence the growth of the Ni–P film.[38] In the Ni–P films fabricated by conventional ELP in our current experiments, the activation processing roughened the surface and nodule growth was confirmed. Nodule suppression is only attainable when the abovementioned factors exert their effects at the reaction site of the plating. That is, the growth suppression factor of the plating reaction and the state of the diffusion layer that conveys the film onto the substrate must both be influenced. ELP-SCE differs from the conventional method in three ways: the stirring speed, the addition of the surfactant for emulsion formation, and the decrease of the pH by the CO_2 dissolution in the plating solution. Henceforth, we will also need to consider

how the collision phenomenon influences the plating film of the CO_2 phase. We will need to collect more evidence to formulate a detailed mechanism for our process. Even so, our experiments have demonstrated that ELP-SCE produces more outstanding results than conventional ELP, forming thin films with high smoothness and superb uniformity.

2.1.5. Conclusion

This chapter has proposed ELP-SCE, a hybrid technique combining ELP and supercritical fluid technology. The ELP reactions are carried out in an emulsion of sc-CO_2 and an ELP solution with surfactant. ELP-SCE formed a uniform Ni–P film free from the pinholes that typically form from the hydrogen bubbles produced by the electrolysis of water, and free from the nodules that form from the nuclear growth in the ELP reaction.

2.2. Direct observation of nodule growth on electroless Ni-P deposition in supercritical CO_2 emulsion

2.2.1. Introduction

The plated film obtained by ELP-SCE was extremely uniform, smooth and free from pinholes and nodules. The film growth speed of ELP-SCE was slower than the conventional ELP. It is reported that an effect of pulse electroplating-like mechanism by adsorption and desorption of the supercritical CO_2 (sc-CO_2) phase from the plated film, called as "Periodic-Plating-Characteristic (PPC)" is a cause in the smoothing mechanism of the electroplating using a supercritical carbon dioxide emulsion (EP-SCE).[22] PPC might not be the only cause of film smoothing and nodule suppression in ELP-SCE since the film formation mechanisms of electroplating and ELP are different, though the nodule formation of ELP-SCE can be affected by fast cycle of adsorption and desorption of dispersed CO_2 phases to a minute convex part, and for the growth to be suppressed.

In addition, PPC effect itself cannot completely explain the effect of higher P content in Ni-P film by ELP-SCE, and the film growth speed is slower than conventional ELP. As one of the factors of the phenomenon of ELP-SCE, CO_2 dissolves in the plating solution and causes decrease of the pH. When the pH of the plating solution decreases, it is expected to cause P content to increase in the plated film and decrease in the film growth speed.[33] Thus, in previous study we discussed that the increase of the proton concentration in the plating solution caused the effect of suppression of nodule growth.[47] However, it is necessary to clarify not only by an indirect method of observing the surface of the plated film via SEM or AFM, but also a direct method of observing growth of one nodule, in order to discuss the suppression mechanism of nodule growth of ELP-SCE clearly. Moreover, the slow film growth speed of ELP-SCE cannot be explained by only making a low pH plating solution. When a plated film fabricated by ELP in the pH=4.0 solution alone with agitation at the same speed used in ELP-SCE, the formation of the plated film was insufficient. For ELP-SCE, the sc-CO_2 phase distributed in the plating solution causes viscosity of plating solution to be low, and, as a result, plating under a high-speed agitation was enabled. This means

http://dx.doi.org/10.5772/54070

thickness of diffusion layer close to surface of substrate and transport property of reactive materials at surface of substrate for ELP-SCE is different from conventional method.

In this chapter, we discuss what influences the characteristic reaction field of ELP-SCE to the plated film growth. In addition, a novel direct observation of nodule is proposed to clarify the nodule suppression mechanism of ELP-SCE. [48] At first, the Ni-P plated film is plated on Cu substrate by the conventional ELP method, and then re-plating by ELP-SCE or conventional ELP method is conducted on the Ni-P plated film in which nodules were formed by conventional ELP. Moreover, morphology of the nodules at a selected position in the Ni-P plated film is compared before and after the re-plating.

Chemicals	
Nickel chloride	9.0%
Sodium hyphosphite	12.0%
Complexing agent	12.0%
Ion-exchange water	67.0%
pH	5.3
Bath temperature	353K

Table 3. Bath composition and operating conditions of electroless Ni - P films

2.2.2. Base Ni-P (BNP) film preparation for direct observation of nodule

The substrate was a film of 99.99% pure copper measuring 10×20 mm (Mitsubishi Shindoh Co., Ltd.). The plated film was made by using the ELP solution shown in 2.1.2 at temperature 353K and reaction time 5 minutes. Process procedures from step 1 to step 8 (Pretreatment-A) was shown in Table 3. The activation agent, the degreasing agent and the ELP solution were purchased from the Okuno Chemical Co., Ltd. The plating solution was kept in a glass beaker in a temperature-controlled water bath agitated with a magnetic agitator and a cross-magnetic stirrer bar. Agitation speed was 50 rpm. The substrate was inserted to the beaker by stainless steel wires. A lot of nodules were formed on the surface for the plated film made with this condition, and the phosphorus content was 14wt% (Fig.26). The plated film is amorphous in as deposited condition and strongly support the observations made from X-ray diffraction (XRD) measurements (Fig.27). When plating was performed again, influence from the substrates is a little because it is an amorphous plated film. Thereafter, the Ni-P film made under this process condition is called base Ni-P film (BNP film).

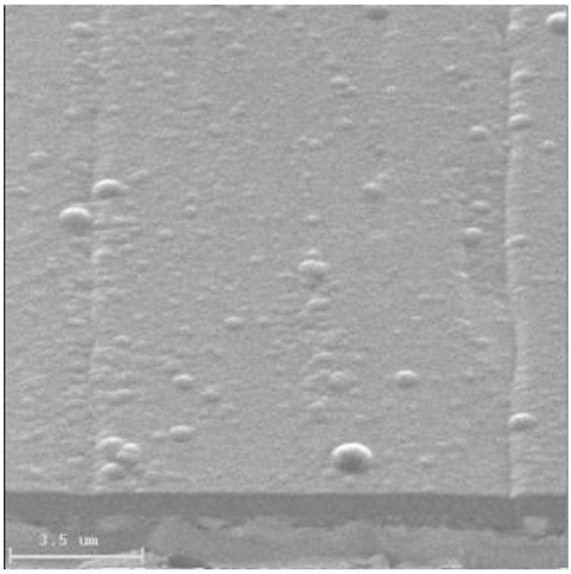

Figure 26. SIM image of Ni-P film by conventional ELP at 353 K and atmospheric pressure for 5min (with a film thickness of 0.8 μm).

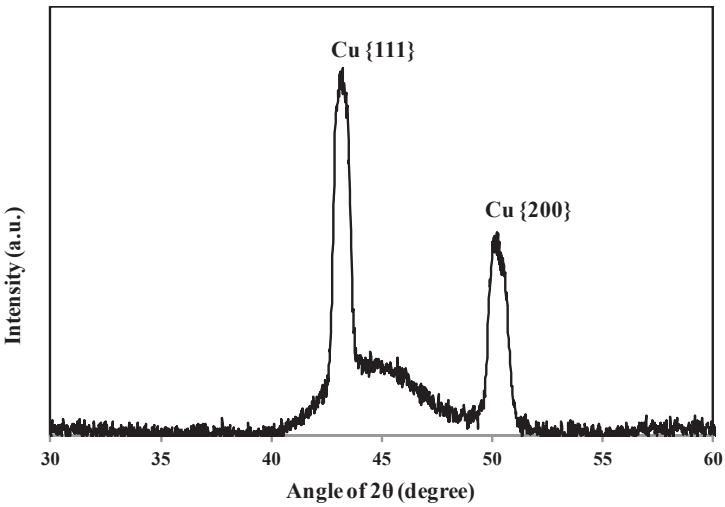

Figure 27. XRD spectrum of Ni-P film plated from conventional ELP at 353K and atmospheric pressure for 5 min.

http://dx.doi.org/10.5772/54070

A rectangular shape shown in Fig.28. was fabricated by focused ion beam system (FIB) (accelerating voltage 40kV) on the surface of BNP film. The fabricating area was made by four rectangles of 50×20 μm to make a square observation area of 50×50 μm. The fabrication program was set so that the gallium (Ga) ion beam was not irradiated to the observation area to prevent influence from irradiated Ga ion of FIB to the plated Ni-P film growth at the observation area. The observation area was measured by atomic force microscopy (AFM) before re-plating, and nodules that become observation candidates were decided on the observation area.

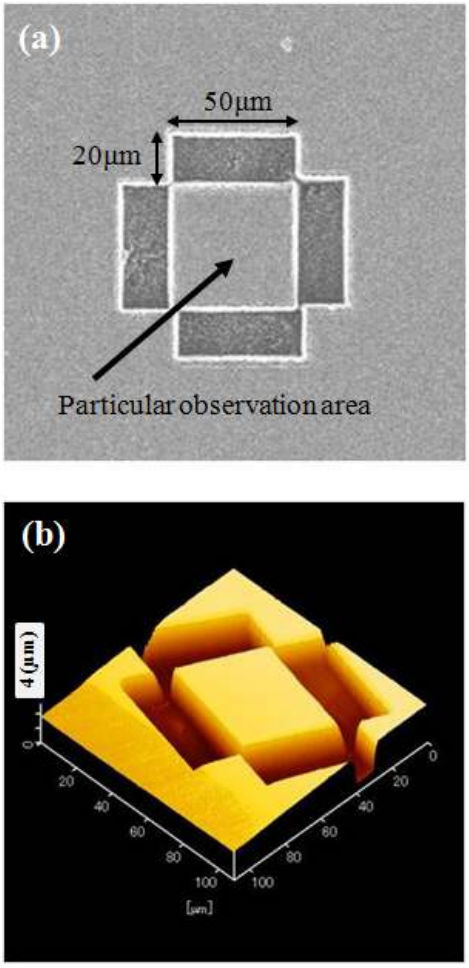

Figure 28. a) SIM and (b) AFM image of rectangular shaped Ni-P film plated by conventional ELP at 353 K and atmospheric pressure for 5min.

The activation treatment using Pd has a big influence on the surface morphology of plated film. This is undesirable to observe the morphological change of the fine nodules[39]. In this study, a pretreatment for the re-plating on the rectangular shaped BNP film was processed in order from step 1 to 6 of Table 4 (Pretreatment-B). In the result of the surface texture measuring instrument, Ra of the plated film was 0.029 μm before and after the pretreatment-B, and the AFM measurement result did not have a substantial change in the surface morphology either (Fig. 29).

Step		Solution composition	Temperature(K)	Duration(min)
1	Cleaning-1	Aceton with ultrasonic cleaning	298	15
2	Cleaning-2	Deionized water	298	1
3	Degreasing	Sodium metasilicate (91.0%)	323	1
		Sodium alkylbenzene sulphonate (5.1%)		
		Surfactant (3.9%)		
4	Rinsing	Deionized water	298	1
5	Acid solution treatment	HCl (10.0%)	298	1
		Ion-exchanged water (90.0%)		
6	Rinsing	Deionized water	298	1
7	Activation	Hydrogen chloride (18.0%)	303	1
		Palladium chloride (0.04%)		
		Ion-exchanged water (81.96%)		
8	Rinsing	Deionized water	298	1

Table 4. Composition of solutions and producers of catalyzing process.

2.2.3. ELP-SCE on pretreated BNP film and on pretreated copper substrate

The rectangular shaped BNP film after pretreatment-B was plated by the conventional ELP and ELP-SCE again respectively. The conventional ELP was the same as the fabrication condition of BNP film. Details on the apparatus and plating method of ELP-SCE can be found in 2.1.2. The observation area after re-plating was measured by AFM, and morphology change of the nodule was analyzed. For re-plating, not only rectangular shaped BNP film after pretreatment-B but also the copper substrate after pretreatment-A was performed regardless of each plating method.

2.2.4. Material characterization

Focused ion beam system (FIB, FB-2100, Hitachi High-technologies Co., Ltd.) has scanning ion microscope (SIM). The liquid-metal ion sources of this instrument used Ga ion sources. SIM was used to observe the surfaces of the plated Ni-P films. A cross section of the plated Ni-P film was fabricated by FIB and the thickness of the plated film could be measured directly from the SIM image on the screen. Moreover, FIB was used for fabricating of the area for carrying out direct observation of the nodule growth. The phosphorous composition of

http://dx.doi.org/10.5772/54070

the base film was measured by an FESEM (S-4300SE, Hitachi High-technologies Co., Ltd.) equipped for energy-dispersive X-ray spectroscopy (EDX). An accelerating voltage of 20 kV with a collecting time of more than 300 s was applied. The surface morphology of plated film was examined using an atomic force microscopy (AFM, SPA-400, Seiko Instruments., Inc.) with a calibrated 20 μm xy-scan and 10 μm z-scan range PZT-scanner. A surface texture measuring instrument (Surfcom 480A, Tokyo Seimitsu Co., Ltd.) with a diamond-tipped detector (2 μm tip radius) was used to measure the average surface roughness (Ra) to a minimum resolution of 1 nm for height (height measurement range: 80 μm). The average Ra was calculated from measurements at three points. 2θ-ω X-ray diffraction (XRD) analysis was performed at room temperature (RT, 298 K) using a PANalytical X'pert Pro Galaxy system equipped with an X'celerator module. The X-ray source was CuKα, and the tube voltage and the current are 45 kV and 40mA, respectively.

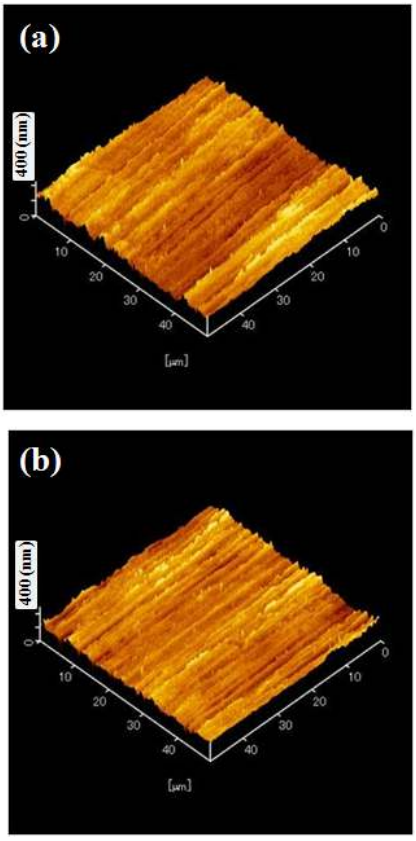

Figure 29. AFM image of (a) Ni-P film by conventional ELP at 353 K and atmospheric pressure for 5min, and (b) After pretreatment-B.

2.2.5. Direct observation of nodule growth in conventional method

Copper substrate after pretreatment-A performed with the re-plating procedure had 0.8 μm of the plated film thickness, and it showed a lot of nodules as that of the BNP film as shown in Fig. 30 (1-a). This means that decomposition of a plating bath did not occur, when re-plating is performed. Film thickness increased from 0.8 μm to 1.7 μm as a result of re-plating on BNP film after pretreatment-B by conventional ELP, and the number of nodules on the surface increased from the initial state as shown in Fig. 30 (1-b). It was possible to re-plating on BNP film with Pretreatment-B. Also, surface observation and film thickness of the plating films by the ELP-SCE and the conventional method using the plating solution with adjusted pH were shown in Figs. 30 (2-a), (2-b), (3-a), and (3-b). The stability of the plating solutions in each method were also confirmed by the observations of the plated surfaces. The plated film thickness is 0.6 μm, and the film has grown up on the copper substrate after Pretreatment-A set up simultaneously (Fig. 30 (2-a)). The film became a smooth film, although there were ditches resulted from the polishing ditches of the copper substrate. The change from initial film thickness of 0.8 μm could not be observed by SIM observation as a result of re-plating on BNP film after Pretreatment-B by ELP-SCE (Fig. 30 (2-b)). The phenomenon in Fig. 30 (2-b) is not peculiar and it also happens when the Ni-P film is obtained after Pretreatment-B without Pd activation and re-plated with low pH bath. A similar phenomenon was confirmed for the re-plating with conventional electroless plating adjusted to pH=4.0 by adding HCl (10wt%). The film was formed as for the copper substrate after Pretreatment-B (Fig. 30 (3-a)) but the film growth was difficult to be confirmed by the SIM observation from Fig. 30 (3-b).

The AFM observation of the BNP film fabricated by FIB before and after re-plating with conventional ELP was shown in Fig. 31. Before re-plating, the film was measured with AFM while raising the magnification from Fig. 31 (1-a) to (1-c), and nodules at a specific position were decided by three places. After re-plating, the change in the morphology of the specific nodule was observed with AFM from Fig. 31 (2-a) to (2-c). The height of nodule before re-plating was 40 nm or less, and the width was about 500 nm. The measurement of the width of nodule was conducted along the direction of the dotted line arrow along the ditch in Fig. 31 (1-d) and (2-d). The shape of nodule was not changed as the film thickness increased to twice that of the initial thickness. The prior growth of nodules can be considered to come from spherical diffusion layer surrounding the neighboring nodule cores on the surface. The localized c oncentration by spherical diffusion occurs at the convex part when the thickness of the diffusion layer is the same or thicker than that of the convex part on the surface, and the thickness of the diffusion layer in neighborhood on the plated film greatly influences the surface-roughness of the plated film.[49,50] The thickness of typical Nernst diffusion layer was reported to be about 0.2 mm, and thickness could be about 0.02 mm when agitation is added.[49] In this experimental condition, it was considered that the Nernst diffusion layer was larger than enough to the size of these nodules in resulting the spherical diffusion[51], and led to a surface morphology like Fig. 31 (2-d). Moreover, this evaluating method is an effective direct observation method to study the growth mechanism and the surface morphology of the plated film including nodule at a specific position.

http://dx.doi.org/10.5772/54070

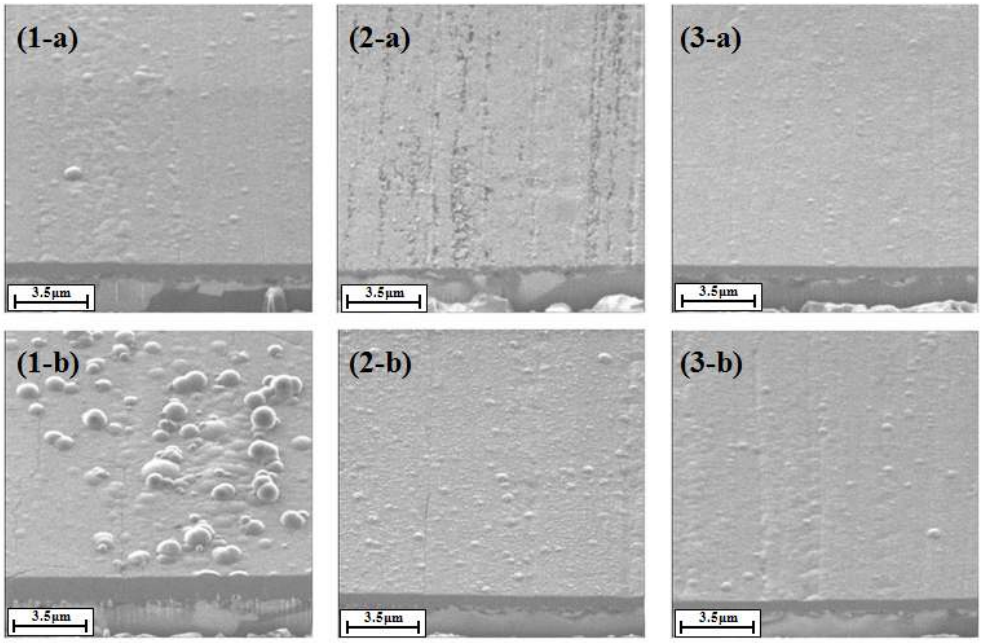

Figure 30. SIM image of Re-Ni-P films plated on the Cu substrate by (1-a) conventional ELP at 353 K and atmospheric pressure for 5 min, (2-a) ELP-SCE at 353 K and 15MPa for 180 min and (3-a) conventional ELP at 353 K and atmospheric pressure for 20 min and pH of plating solution is 4.0. (b) means SIM image that plates the BNP film being processed for pretreatment-A put at the same time as each (a) samples.

The effect of PPC proposed with EP-SCE and the mechanical agitation are the causes for decrease in the thickness of the diffusion layer of ELP-SCE. PPC for the sc-CO_2 phase to repeat adsorption and desorption on the surface of the plated film could appear as similar as that of the pulse electro deposition (PED).[52] Actually, Rahman have succeeded by using the effect of PPC in the sc-CO_2 emulsion and the perfluorocarbon surfactant in forming the porous film.[30] Size of the pores are roughly several μm or less depends on the size of the sc-CO_2 phase, which can be controlled by pressure, the amount of CO_2, and the amount of the surfactant. Moreover, the influence of the mechanical agitation is an important factor in the diffusion layer control. In the PED, the mechanical agitation and the duty cycle are optimized, and the thickness of the diffusion layer is controlled.[53] In ELP-SCE, the plating reaction field is made by making sc-CO_2 and the plating solution in an emulsion to lowered the viscosity. This gives the possibility to exert a difference in influence from the mechanical agitation like the conventional on the growth of the plated film.

2.2.6. Suppression of nodule growth in ELP-SCE

An extraordinary effect was confirmed for the morphological change of nodule (Fig. 32). This is the first report on of direct observation of the effect of nodule growth suppression by

ELP-SCE. Decrease in size of nodules and initiation of nucleation on the surface at random were observed though the plated film as the film grew up. The ditch parts were on the substrate before re-plating, which were filled after re-plating as shown in Fig.32 Random generation of the refined nucleus and leveling effect are similar to the phenomenon that happens because of PPC.[22] The effect of the leveling of ELP-SCE could be caused by the fact that the thickness of the diffusion layer is as thin as the size of these nodules. On the other hand, we discussed the influence of the proton for the growth suppression of nodule in the previous chapter. The re-plating experiment was done by conventional ELP that used the plating bath with pH adjusted to 4.0 by adding HCl (10 wt%) to confirm the influence of diffusion layer thickness of ELP-SCE and the proton. New nodules were observed to be hardly formed after re-plating as shown in Fig. 33. The plated film was observed to be from 183 nm to 254 nm as a result of measuring the width of ditch before and after re-plating, because of this re-plating. The growth of the convex part was suppressed under a plating condition even when it was thought that there was a thicker diffusion layer where spherical diffusion happened. However, all peculiar phenomena of ELP-SCE were not able to be shown. That is, the thickness change in the diffusion layer in addition to the influence of the proton greatly influences in ELP-SCE.

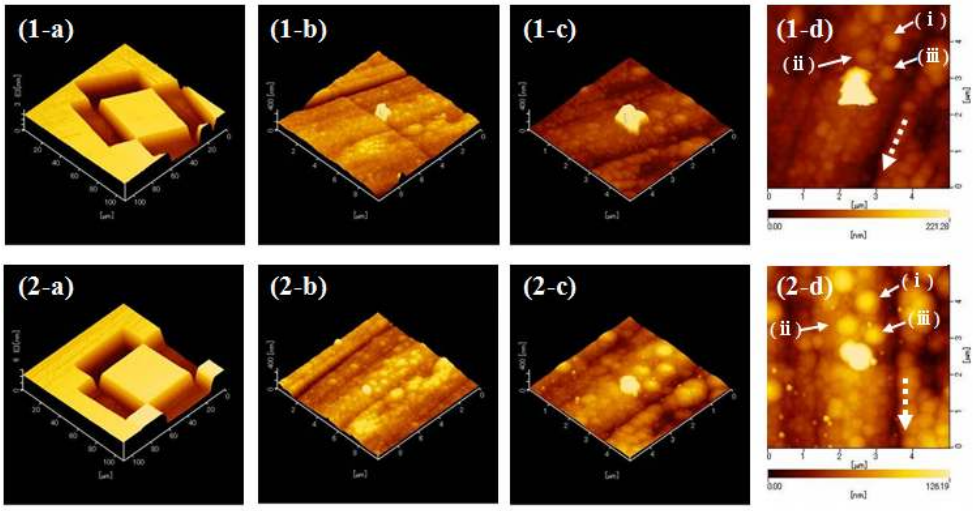

Figure 31. AFM images (1-a, b, c, d) of rectangular shaped Ni-P film plated by conventional ELP at 353 K and atmospheric pressure for 5 min, and (2-a, b, c, d) of re-plated Ni-P film plated by conventional ELP at 353 K and atmospheric pressure for 5 min on the (1-a) film. The magnification rises from (a) to (c). (d) is 2D image of (c). The dotted arrow indicates the direction where the width of nodules was measured.

http://dx.doi.org/10.5772/54070

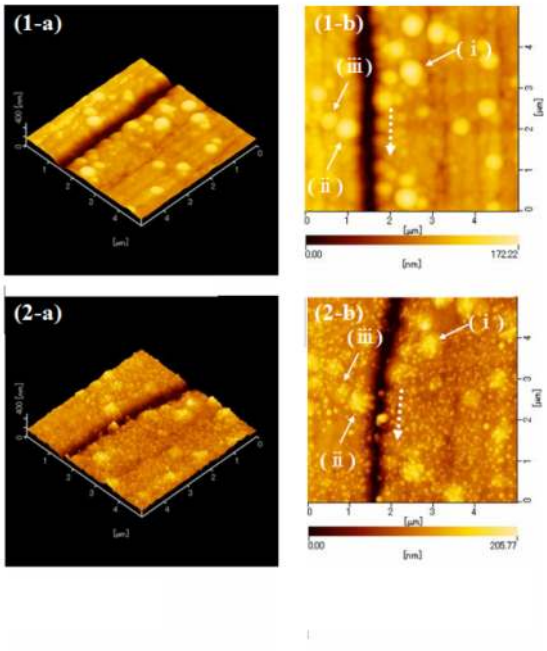

Figure 32. AFM images (1-a) of rectangular shaped Ni-P plating film plated by conventional ELP at 353 K and atmospheric pressure for 5min, and (2-a) of re-plated Ni-P film plated by ELP-SCE at 353 K and 15 MPa for 180 min on the (1-a) film. (number-b) is 2D image of (number-a). The dotted arrow indicates the direction where the width of nodules was measured.

Two influences mentioned above on the plating reaction field might be the formation factors of the refined nuclei observed. In the PED, the nucleation is promoted because the plating reaction can be performed at high overpotential, and it becomes easy for a minute crystallization to occur. On the other hand, the ELP that was not applied by the external power is the base reaction in ELP-SCE, and the electron necessary for the nucleation is only supplied by the reducing agent oxidized on the plated film. Also, crystallization overpotential that is higher than nuclear growth are necessary for the nucleation in the electrocrystallization.[54] Therefore, it will be necessary to supply a large amount of reducing agents to a reaction surface in ELP-SCE. The small film growth speed of ELP-SCE might have been caused by the reaction filed where the nucleation occur more frequently than nuclear growth. It causes high P content with plated film by ELP-SCE, moreover, because not only the reducing agent but also other reactive species such as the metal ions and protons are supplied easily voluminously so far because of PPC and the mechanical agitation.

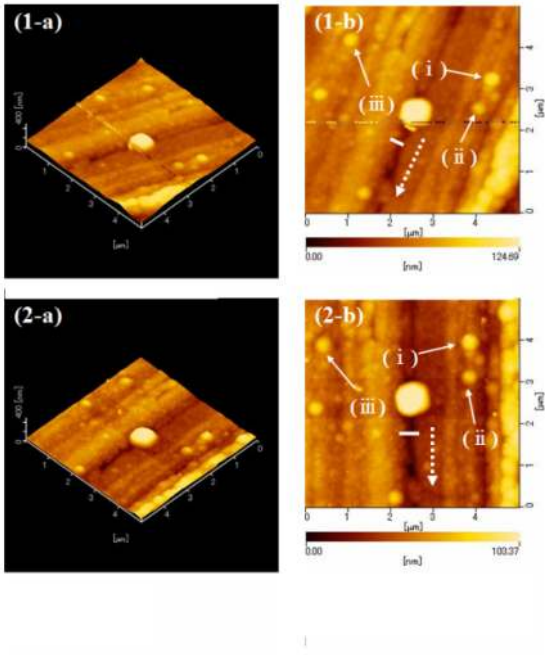

Figure 33. AFM images (1-a) of rectangular shaped Ni-P plating film plated by conventional ELP at 353 K and atmospheric pressure for 5min, and (2-a) of re-plated Ni-P film plated by conventional ELP at 353 K and atmospheric pressure for 20 min and pH 4.0 of plating solution on the (1-a) film. (number-b) is 2D image of (number-a). The dotted arrow indicates the direction where the width of nodules was measured

2.2.7. Conclusion

We examined a direct observation of selected nodule growth in ELP reaction using AFM on a square sample substrate of 50×50 μm fabricated by FIB. The Ni-P plated film is plated by the conventional method and ELP-SCE again on the Ni-P plated film with nodule formed. Changes in fine nodules and other areas at a specific position in the surface morphology were compared before and after the re-plating. In ELP-SCE, the dominant growth of nodules was suppressed and the nucleation occurred on the other surface of the nodules, although the convex part of nodules grew dominantly in conventional ELP using the electrolyte only.

Author details

Masato Sone*, Tso-Fu Mark Chang and Hiroki Uchiyama

*Address all correspondence to: msone@pi.titech.ac.jp

Precision & Intelligence Laboratory, Tokyo Institute of Technology, Yokohama, Japan

References

[1] Clifforo T. Fundamentals of supercritical fluids. United Kingdom: Oxford University Press; 1999.

[2] McHugh M, Krukonia V. Supercritical fluid extraction: principles and practice. United States of America: Butterworth Publishers; 1986.

[3] Shimoyama Y, Ogata Y, Ishibashi R, Iwai Y. Drying processes for preparation of titania aerogel using supercritical carbon dioxide. Chem. Eng. Res. Des. 2010; 88(10): 1427-1431.

[4] Gad-el-Hak M. The MEMS Handbook. Boca Raton, Fla.: CRC, Taylor & Francis; 2006.

[5] Schultze JW, Bressel A. Principles of electrochemical micro- and nano-system technologies. Electrochima Acta 2010; 47(1): 3-21.

[6] Ke J, Su W, Howdle SM, George MW, Cook D, Perdjon-Abel M, Bartlett PN, Zhang W, Cheng F, Levason W, Reid G, Hyde J, Wilson J, Smith DC, Mallik K, Sazio P. Electrodeposition of metals from supercritical fluids. P. Natl. Acad. Sci. 2009; 106(35): 14768-14772.

[7] Tsai WL, Hsu PC, Hwu Y, Chen CH, Chang LW, Je JH, Lin MH, Groso A, Margaritondo G. Electrochemistry: Building on bubbles in metal electrodeposition. Nature (2002); 417: 139.

[8] Howdle SM, Bagratshvili VN. The effects of fluid density on the rotational Raman-spectrum of hydrogen dissolved in supercritical carbon-dioxide. Chem. Phys. Lett. (1993); 214: 215-219.

[9] Darr JA, Poliakoff M. New directions in inorganic and metal-organic coordination chemistry in supercritical fluids. Chem. Rev. (1999), 99: 495-541.

[10] McClain JB, Betts DE, Canelas DA, Samulski ET, DeSimone JM, Londono JD, Cochran HD, Wignall GD, Chillura-Martino D, Triolo R. Design of nonionic surfactants for supercritical carbon dioxide. Science (1996); 274(5295): 2049-2052.

[11] Johnston KP, da Rocha SRP. Colloids in supercritical fluids over the last 20 years and future directions. J. Supercrit. Fluids (2009); 47(3): 523-530.

[12] Lee CT Jr, Ryoo W, Smith PG Jr, Arellano J, Mitchell DR, Lagow RJ, Webber SE, Johnston KP. Carbon dioxide-in-water microemulsions. J. Am. Chem. Soc. (2003);125(10): 3181-3189.

[13] Yoshida H, Sone M, Wakabayashi H, Yan H, Abe K, Tao XT, Mizushima A, Ichihara S, Miyata S. New electroplating method of nickel in emulsion of supercritical carbon dioxide and electrolyte solution to enhance uniformity and hardness of plated film. Thin Solid Film (2004); 446(2): 194-199.

[14] Yan H, Sone M, Sato N, Ichihara S, Miyata S. The effects of dense carbon dioxide on nickel plating using emulsion of carbon dioxide in electroplating solution. Surf. Coat. Tech. (2004); 182: 329-334.

[15] Wakabayashi H, Sone M, Sato N, Takada Y, Yan H, Abe K, Ichihara S, Miyata S. Nano-grain structure of nickel films prepared by emulsion plating with dense carbon dioxide. Surf. Coat. Tech. (2005); 190(2-3): 200-205.

[16] Jeong DH, Gonzalez F, Palumbo G, Aust KT, Erb U. The effect of grain size on the wear properties of electrodeposited nanocrystalline nickel coatings. Scr. Mater. (2001); 44(3): 493-499.

[17] Hugh GD, Smith SD, Pande CS, Johnson HR, Armstrong RW. Hall-petch strengthening for the microhardness of twelve nanometer grain diameter electrodeposited nickel. Scr. Metall. (1986); 20(1): 93-97.

[18] Rahman MdZ, Sone M, Eguchi M, Ikeda K, Miyata S, Yamamoto T. Wear properties of nickel coating film plated from emulsion with dense carbon dioxide. Surf. Coat. Tech. (2006); 201(3-4): 606–611.

[19] Chung ST, Tsai WT. Nanocrystalline Ni-C electrodeposits prepared in electrolytes containing supercritical carbon dioxide. J. Electrochem. Soc. (2009); 156(11): D457-D461.

[20] Rashidi AM, Amadeh A. The effect of saccharin addition and bath temperature on the grain size of nanocrystalline nickel coatings. Surf. Coat. Tech. (2009); 204(3): 353-358.

[21] Bakonyi I, Tóth-kádár E, Pogány L, Cziráki Á, Geröcs I, Varga-Josepovits K, Arnold B, Wetzigdeh K. Preparation and characterization of d.c.-plated nanocrystalline nickel electrodeposits. Surf. Coat. Tech. (1996); 78(1-3): 124-136.

[22] Chang TFM, Sone M. Function and mechanism of supercritical carbon dioxide emulsified electrolyte in nickel electroplating reaction. Surf. Coat. Tech. (2011); 205(13-15): 3890-3899.

[23] Chang TFM, Sone M, Shibata A, Ishiyama C, Higo Y. Bright nickel film deposited by supercritical carbon dioxide emulsion using additive-free Watts bath. Electrochim. Acta (2010); 55(22): 6469-6475.

[24] Dhanuka VV, Dickson JL, Ryoo W, Johnston KP. High internal phase CO_2-in-water emulsions stabilized with a branched nonionic hydrocarbon surfactant. J. Colloid Interf. Sci. (2006); 298(1): 406-418.

[25] da Rocha SRP, Psathas PA, Klein E, Johnston KP. Concentrated CO_2-in-water emulsions with nonionic polymeric surfactants. J. Colloid Interf. Sci. (2001); 239(1): 241-253.

[26] Vesovic V, Wakeham WA. The Transport Properties of Carbon Dioxide. J. Phys. Chem. Ref. Data (1990); 19(3): 763-808.

[27] Yuan X, Wang Y, Sun D, Yu H. Influence of pulse parameters on the microstructure and microhardness of nickel electrodeposits. Surf. Coat. Tech. (2008); 202(9): 1895-1903.

[28] Choo RTC, Toguri JM, El-Sherik AM, Erb U. Mass transfer and electrocrystallization analyses of nanocrystalline nickel production by pulse plating. J. Appl. Electrochem. (1995); 25(4): 384-403.

[29] El-Sherik AM, Erb U, Page J. Microstructural evolution in pulse plated nickel electrodeposits. Surf. Coat. Tech. (1997); 88(1-3): 70-78.

[30] Rahman MdM, Sone M, Uchiyama H, Sakurai M, Miyata S, Nagai T, Higo Y, Yamamoto T. Novel porous film by electroplating with an emulsion of supercritical CO_2. Surf. Coat. Tech. (2007); 201(16-17): 7513-7518.

[31] Lee CT Jr, Ryoo W, Smith PG Jr, Arellano J, Mitchell DR, Lagow RJ, Webber SE, Johnston KP.Carbon dioxide-in-water microemulsions. J. Am. Chem. Soc. (2003);125(10): 3181-3189.

[32] Adkins SS, Chen X, Chan I, Torino E, Nguyen QP, Sanders AW, Johnston KP. Morphology and stability of CO_2-in-water foams with nonionic hydrocarbon surfactants. Langmuir (2010); 26(8): 5335-5348.

[33] Mallory G O, Hajdu J B, *Electroless Plating: Fundamentals and Applications*, American Electroplaters and Surface Finishers Society, Orlando, FL; (1990).

[34] Tracton A A, in *Coatings Technology Handbook*, 3nd ed., Vakelis A, Editor, p. 27-1, CRC Press Taylor & Francis Group, New York;(2006).

[35] Uchiyama H, Sone M, Ishiyama C, Endo T, Hatsuzawa T, Higo Y, Uniform Ni-P Film using an Electroless Plating Method with an Emulsion of Supercritical Carbon Dioxid.e J.Electrochem.Soc, (2007); 154; E91-E94.

[36] Imai Y, What is Supercritical Fluid ?, *Hyomen Gijutsu*, 2005; 56, 74-78.

[37] Watanabe H, Honma H, brication of Nickel Microbump on Aluminum using Electroless Nickel Plating *J. Electrochem. Soc.*, (1997); 144; 471.

[38] Chang S Y, Hsu C J, Fang R H, Lin S J, Electrochemical Deposition of Nanoscaled Palladium Catalysts for 65 nm Copper Metallization *J. Electrochem. Soc*., (2003); 150; C603.

[39] Tsunoda T, Nagashima H, Nishinakayama H, Watanabe H, Honma H, Effect of Direct Electroless Nickel Plating Process on Surface Morphology of Nickel Plating, *Hyomen Gijutsu*, (2005);56; 463-467.

[40] Paunovic M, Schlesinger M, *Fundamentals of Electrochemical Deposition*, 2nd ed., John Wiley & Sons, Hoboken, NJ; (2006).

[41] Nakamaru Y, Joya T, Tashiro K, Honma H, Reduction of Pit and Nodule Defects on Thick Electroless Nickel Plating Film, *Hyomen Gijutsu*, (2009); 60; 661-667.

[42] Tashiro K, Yamamoto S, Hashimoto Y, Kawashima S, Honma H, Initial deposition morphologies of electroless nickel-phosphorus plating on a nonconductor and a conductor, *Hyomen Gijutsu,* (2002); 53; 459-465.

[43] Cheong W J, Luan B L, Shoesmith D W, The effects of stabilizers on the bath stability of electroless Ni deposition and the deposit, *Appl. Sur. Sci*., (2004); 229; 282-300.

[44] Jacobs J W M, Rikken J M G, Oxygen-Diffusion-Size Effect in Electroless Metal Deposition, *J. Electrochem. Soc*., (1988); 135; 2822-2827.

[45] Chandrasekar M S, Pushpavanam M, Pulse and pulse reverse plating—Conceptual, advantages and applications, *Electrochim. Acta*., (2008); 53; 3313-3322.

[46] Hsu H H, Yeh J W, Lin S J, Repeated 3D Nucleation in Electroless Cu Deposition and the Grain Boundary Structure Involved, *J. Electrochem. Soc*., (2003); 150, C813-C815.

[47] Uchiyama H, Shibata A, Sone M, Higo Y, Effects of CO_2 on Ni-P Electroless Plating in an Emulsion of Supercritical CO_2, *J.Electrochem.Soc, (*2010);157; D550-D552.

[48] Uchiyama H, Endo T, Sone M, Direct Observation of Nodule Growth on Electroless Ni-P Deposition in Supercritical CO_2 Emulsion, *J.Electrochem.Soc,* (2012); 159; D114-D118.

[49] Paunovic M, Schlesinger M, *Fundamentals of Electrochemical Deposition*, 2nd ed., John Wiley & Sons, Hoboken, NJ; (2006).

[50] Despic A R, Popov K I, *J. Appl. Electrochem*., (1971); 1; 275.

[51] Chou Y H, Sung Y, Liu Y M, Pu N W, Ger M D, Defect-Free Copper Filling Using Nonisothermal Electroless Deposition with Fluorocarbon Surfactant, *J. Electrochem. Soc*., (2008); 155; D791.

[52] Lam T L, Koike A, Ohno I, Haruyama S, *J. Met. Finish. Soc. Jpn*., (1983); 34; 428.

[53] Kaishev R, Mutaftschiev B, An International Journal of the Science of Corrosion and Protection of Metals, *Electrochim. Acta*., (1965); 10; 643-716